12-2011

IN VITRO STUDY OF FLUID DIODES IN THE PULMONARY VALVE POSITION

John Porcher
Clemson University, jporche@clemson.edu

IN VITRO STUDY OF FLUID DIODES IN THE PULMONARY VALVE POSITION

A Thesis
Presented to
the Graduate School of
Clemson University

In Partial Fulfillment
of the Requirements for the Degree
Master of Science
Mechanical Engineering

---

by
John Clement Porcher
December 2011

Accepted by:
Dr. Richard S. Figliola, Committee Chair
Dr. Donald E. Beasley
Dr. Xiangchun Xuan

ABSTRACT

Every year many people suffer from severe chronic pulmonary insufficiency. Problems that can be incurred include the valve becoming stenotic, where it inhibits antegrade flow, and incompetent, allowing retrograde flow. When either of these conditions occurs with great severity, it is often necessary for the native valve to be replaced. There are no acceptable, permanent solutions currently available for a pulmonary valve replacement. Previous research, based on regurgitant fraction and transvalvular gradient, has indicated that a fluid diode could possibly serve as a permanent valve replacement solution. This study investigated the effectiveness of a diode to reduce the workload of a right ventricle while maintaining a tolerable regurgitant fraction and transvalvular pressure gradient. Three different diode geometries were compared to each other and also to a comparable stenosis and a blank annulus. The valve prototypes were tested in two positions in the mock pulmonary circulatory system (MPCS), immediately in the right ventricle outflow tract (RVOT) and also 3 cm downstream, in the pulmonary artery test section. The results of this study indicate that while all three of the diode designs performed very similarly to each other in each set of tests, the performance of the diodes varied greatly between the two positions in which they were tested. The diodes tested in the RVOT significantly reduced regurgitant fraction (RF), transvalvular gradient (TVG), and ventricular work as compared to the stenosis. However, the diodes demonstrated no significant reduction in TVG or ventricular work as compared to the stenosis or the blank annulus when placed within the pulmonary artery.

ACKNOWLEDGMENTS

I would like to thank the defense committee members Dr. Figliola, Dr. Beasley, and Dr. Xuan for their guidance in this project. I am especially grateful to Dr. Figliola for being an excellent advisor. I would also like to thank the members of the research team who assisted my progress: Dr. Tim Conover, who helped me the most; Dr. Tiffany Camp, who bequeathed to me the lab and everything that would become my project; and John Chiulli, who, although busy with his own research, was of assistance on many occasions. I would like to thank Michael Justice, Jamie Cole, Stephen Bass, and also the guys at Machining and Technical Services (MTS) for their assistance in building and machining parts for my systems.

I especially would like to thank my folks for their prayers and support. I know I would not be where I am today without both of them. I am grateful to the many friends and family members who also have been there for me. I would like to specifically acknowledge David Sitarski. If I had spent as much time on my research as I spent fishing with him, I would probably have finished a year ago. Every trip was worth it though. I am also grateful to the Aiken family for “adopting” me. Some of their home-cooked dishes rival my own.

TABLE OF CONTENTS

Page

Table of Contents (Continued)

Page

LIST OF FIGURES

List of Figures (Continued)

List of Figures (Continued)

Figure Page

LIST OF TABLES

LIST OF ACRONYMS

CO	cardiac output
EDPVR	end-diastolic pressure-volume relationship
ESPVR	end-systolic pressure-volume relationship
FFT	fast Fourier transform
HR	heart rate
MPCS	mock pulmonary circulatory system
PA	pulmonary artery
PAP	pulmonary artery pressure
PPVI	percutaneous pulmonary valve implantation
PSP	polyamid seeding particles
PVC	pulmonary vascular compliance
PVL	pressure-volume loop
RVP	right ventricular pressure
PVR	pulmonary vascular resistance
RF	regurgitant fraction
RV	right ventricle
RVOT	right ventricular outflow tract
SJMB	St. Jude medical bileaflet
TVG	transvalvular gradient

CHAPTER ONE

INTRODUCTION

Valvular heart disease, which occurs when a heart valve fails to function correctly, is a potentially lethal condition that affects several million people each year. Either one of the heart's four valves may develop a narrowing of the valve opening, which is called mitral, tricuspid, aortic or pulmonic stenosis, depending on which heart valve is effected. Another condition which may occur is valvular insufficiency, when the leaflets of the valve fail to close properly, allowing regurgitant flow during diastole.

Currently, options for patients with stenosed or incompetent heart valves include either no treatment, or implantation of bio-prosthetic or mechanical valves. Without treatment, many of these patients can live somewhat normal adolescent lives. However, as they reach adulthood, often the heart can not keep up with normal activities, and the condition can become fatal. Bio-prosthetic valves implants are not ideal because they last only a decade or two and must then be replaced; they have a tendency to deteriorate even faster when implanted in younger, pre-adult patients (Bloomfield, 2002). Mechanical valves have successfully replaced mitral and aortic valves for many years. However, due to the lower operating pressures of the pulmonary circulation, and the increased tendency for thrombosis to occur on mechanical heart valves in the pulmonary position (Kawachi et al., 1991), current mechanical valves which have been developed for use in the left heart are poorly suited as replacements for pulmonary valves (Ilbawi et al., 1987).

Permanent, effective solutions for pulmonary valve replacements are being sought. One such device being studied is a non-moving preferred resistance device, or

fluid diode. The purpose of this study is to determine the effectiveness of a fluid diode at reducing the work load of a heart with a defective pulmonary valve while controlling regurgitation with reduced pressure gradient, and to study the effects of small changes in the geometry on such performance. An existing mock pulmonary circulatory system (MPCS) from previous research was modified significantly to more accurately match the hemodynamics of the right ventricle and pulmonary artery and to allow for the collection of instantaneous pressure-volume measurements within the ventricle. The study herein couples flow visualization with parametric geometry variation to assess the operational performance of a particular type of diode for use as a pulmonary valve.

Literature Review

The heart is the driving mechanism for the circulatory system. It consists of a right and left atrium and a right and left ventricle and operates as two pumps in series. The right atrium is a holding chamber for the right ventricle, which powers the pulmonary circulation. Similarly, the left atrium is a holding chamber for the left ventricle, which powers the systemic circulation. During systole, the right ventricle contracts, driving blood through the pulmonary artery, through the lungs, and into the left atrium. Simultaneously, the left ventricle contracts, pumping freshly oxygenated blood throughout the rest of the body and into the right atrium. During diastole, as the ventricles relax, the atriums contract slightly and blood flows from them into the respective ventricles, filling them for the next cycle. There are four valves in the heart which facilitate the forward flow of blood. The mitral and tricuspid valves are between the

atrium and ventricle of the left and right heart respectively. The aortic and pulmonary valves are between the left ventricle and aorta and between the right ventricle and pulmonary artery respectively.

When the heart and all its valves are functioning properly, the cardiac output of both ventricles is the same, about 5-25 L/min, depending on whether the subject is at rest or engaged in heavy exercise (Levick, 1995). The average frequency of the heart is 70 beat per minute, also dependent on whether the subject is at rest or exercising (Berne et al., 1992). In a typical heart beat, which lasts about 850 ms, systole begins when the aortic and pulmonary valves open, and lasts about one third of the cycle (Yoganathan et al., 2004).

While the flow rates in each ventricle must remain the same, the working pressures of the two are quite different. The pulmonary and tricuspid valves of the right heart typically only experience 30 mmHg of pressure gradient across their leaflets, while the aortic and mitral valves of the left heart must withstand 100 mmHg and 150 mmHg respectively (Yoganathan et al., 2004). These widely contrasted pressures in the two ventricles are due to the fact that the resistance in the peripheral vessel network of the systemic circulation is approximately ten times the resistance of the pulmonary vessel network (Berne et al., 1992). This resistance that the pulmonary circulation offers the right ventricle is best characterized by the pulmonary vascular resistance (PVR) which is the ratio of the mean pulmonary artery pressure to the mean cardiac output (Weinberg et al., 2004). Mousseaux et al. (1999) found that normal lungs have a PVR between 1 and 5 mmHg/Lpm, with an average of 2.0 mmHg/Lpm. However, patients suffering from

pulmonary hypertension could have a PVR over 20 mmHg/Lpm. Another parameter that greatly affects pulmonary hemodynamics is arterial compliance. As the heart contracts, the increase in pressure causes the arteries to expand. Consequently, as the pressure drops during diastole, the arteries revert to their original state. Pulmonary vascular compliance (PVC) is this change in volume due to the changes in pressures. PVC is characterized by the ratio of the ventricle stroke volume to the arterial pulse pressure. In a study with 35 subjects, Reuben (1971) found that normal patients had an average PVC of about 2.87 ml/mmHg while the PVC of patients suffering from severe pulmonary hypertension could be as low as 0.7 ml/mmHg. However, another study reported values ranging from 4 to 8 ml/mmHg (Slife et al., 1990). Both PVR and PVC vary considerably with activity, and they maintain an inverse relationship (Lankhaar et al., 2008).

There are several congenital and acquired complications that can affect a native heart valve. The two means of failure that are of primary concern in this study are stenosis and regurgitation. Pulmonary stenosis occurs when the pulmonary valve is malformed such that it inhibits forward flow. With a narrow opening, the valve becomes an orifice, creating a pressure gradient across the valve. This increase in pressure causes the ventricle to have to work much harder to maintain a healthy cardiac output. Since the right ventricle can tolerate a mild pressure gradient, a mild stenosis can be ignored. A pulmonary stenosis is considered to be severe if it causes a pressure gradient of 40 mmHg or greater (Alexander, 1998). In the medical field, the term pressure gradient simply refers to the maximum pressure drop across the valve during systole. Often, the leaflets of a stenosed valve fail to close properly, allowing the flow to regurgitate. This is known as

an insufficiency. If the regurgitant flow is severe enough, it will significantly increase the work load on the ventricle and cause the ventricle to dilate. Pulmonary regurgitant flow of 10-30 mL per stroke is considered mild (Tulevski et al., 2003). Therefore, for a typical heart rate of 70 beats per minute and a cardiac output of 5 L/min, any pulmonary regurgitation up to 2.1 L/min, or a regurgitant fraction (RF) of 42%, is considered mild. If either stenosis or insufficiency is severe enough, the valve may need to be replaced.

Currently, the two options for heart valve replacement are bio-prosthetic and mechanical valves. The four types of bioprosthetic valves, the stented procine valve, stented pericardial valve, stentless porcine valve, and homographs have been extensively review by Butany et al. (2003). While these valves function very similarly to the native valve, they lack robustness and longevity. Over time these valves can deteriorate and require additional operations, especially when implanted into younger patients (Fukada et al., 1997). Despite these shortcomings, bioprosthetic valves are the most common replacement for pulmonary valves. There are three types of mechanical valves: caged ball, tilting disk, and bileaflet. Butany et al. produced an extensive review of these valves as well (2003). All of these valves are susceptible to severe problems such as thromboembolic complications, pannus formation, and mechanical failure. As blood flows through a mechanical valve, platelets are disturbed and activated (Harker et al., 1970). These platelets can begin to coagulate and cause thrombus formations to build up on the valve. As the formations continue to grow, they can eventually impede the motion of the valve completely, resulting in valve failure. There is also a risk of thromboembolism, which occurs when a loose piece of thrombus travels downstream and

clogs a blood vessel. To minimize the risk of thrombosis, patients who undergo mechanical heart valve implants must go on anticoagulant therapy. This leads to other medical issues such as the risk of severe, life-threatening hemorrhaging, especially from internal wounds. Deviri et al. (1991) found that almost half of the patients in a study who had a mechanical valve obstructed by thrombus also experienced pannus growth. The bileaflet valve was less-susceptible to obstructions than the tilting disk valve, and these obstructions were just as likely to form on an aortic as on a mitral valve. Pannus is the overgrowth of tissue around the sewing ring and can lead to stenosis and seized leaflets. Mechanical failure is another possible failure mode for mechanical valves. Early models such as the caged ball valves were especial susceptible to failure by the balls swelling or cracking (Butany et al., 2003). While other mechanical valves are susceptible to leaflet cracking or dislodgement, the occurrences of such failures are much rarer, especially for bileaflet valves. Two independent follow-up studies conducted by Chang et al. (2001) and Emery et al. (2003) investigated over 900 recipients of a St. Jude Medical bileaflet valve and found zero mechanical failures.

With proper anticoagulation therapy, the risk of thromboembolic complications is greatly reduced for mechanical valves placed in the aortic or mitral positions. However, due to the lower operating pressures of the right ventricle, mechanical valves in the pulmonary position are much more prone to thrombosis and pannus growth, even with appropriate anticoagulant therapy (Ilbawi et al., 1987). Another concern with placement of mechanical valves in the pulmonary position is mechanical malfunction such as leaflet flutter and failure to close properly. Gohean et al. (2006) found that the lower vascular

resistance in the pulmonary circulation can cause aberrant behavior for both bileaflet and tilting disk valves.

Over the last several years some research has shifted toward the development of percutaneous pulmonary valve implantation (PPVI). With PPVI, valves, which are typically homographs, porcine aortic valves, or bovine jugular venous veins, can be mounted on a stent and inserted in place without the need of open-heart surgery (Lurz et al., 2008). Not all patients are suitable for percutaneous pulmonary valve insertion. Due to limitations on the size of these stented valves, patients must meet artery dimension requirements (Lurz et al., 2009). If the patient's artery has too large a diameter (larger than 22 mm), the device can not be dilated enough to fill the entire vessel, and blood could flow around the stent. Another concern with PPVI is that the stent on which the valve is mounted has a tendency to fracture. In a study of 123 patients, Nordmeyer et al. (2007) found that over 20% of the patients developed a stent fracture within three years of PPVI. In many cases, the fractured stent led to restenosis of the valve, and in one case, separation of fragments and embolization.

Clearly neither bioprosthetic nor mechanical valves are ideal candidates for pulmonary valve replacement. Camp et al. (2007) proposed the concept of a fluid diode as a motionless device to regulate the pulmonary insufficiency. The device, called a fluid diode, offers significantly more resistance to retrograde flow than to antegrade flow. The original design, discussed by Losaw (2004), was inspired by a simple nozzle profile as outlined in the ASME nozzle design manual (Bean, 1971) and the valvular conduit patented by Tesla (1920). The standard nozzle is shown in Figure 1.1.

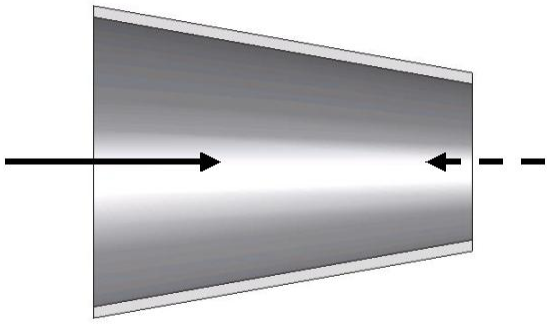

Figure 1.1: Standard nozzle.

Tesla's valvular conduit seen in Figure 1.2 utilizes a series of backflow passages to significantly impede reverse flow while the forward flow is less affected. Forward flow in Figure 1.2 is right to left.

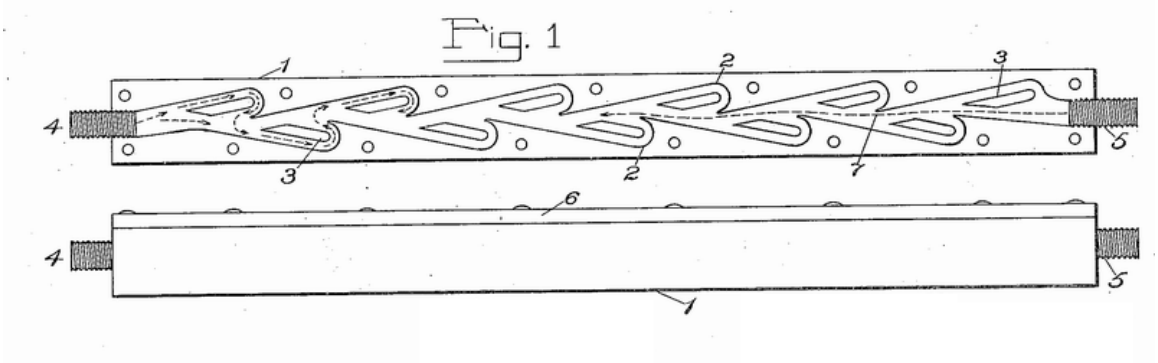

Figure 1.2: Figure 1 from Tesla's valvular conduit (Tesla, 1920).

This idea is carried forward into the diode discussed by Camp et al. (2007). The nozzle allows low resistance flow between the ventricle and the artery during systole, but flow passages increase resistance during retrograde flow of diastole. The resulting diode design is seen in Figure 1.3. Forward flow is from left to right.

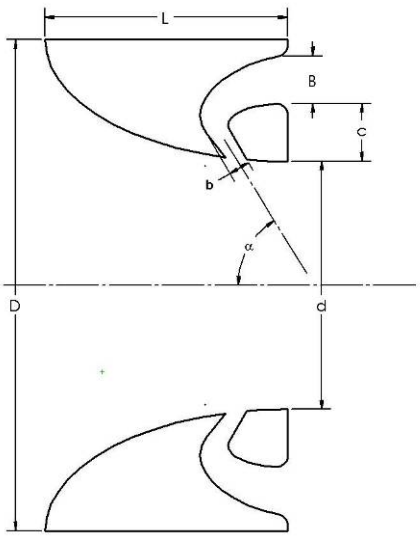

Figure 1.3: Generically dimensioned diode valve (Camp, 2007).

α - impingement angle of backflow channel jet
d – minor orifice diameter
D – major orifice diameter
β - ratio of minor to major orifice diameter, d/D
L – overall length of the diode
b – minor width of backflow channel
B – Major width of backflow channel
c – annular ring width

The design tested by Camp et al. (2007) used a 25 mm tissue annulus diameter. The ratio of inlet diameter *D* to the minor throat diameter *d* was 2 to 1 or a beta ratio, β, of 0.5.

$$\beta = d / D \tag{1.1}$$

Camp (2009) continued the development of the diode by investigating various geometry parameters. An additional design was added which removed the backchannel, resulting in an open-cusped diode. Figure 1.4 shows two SolidWorks models, one with the backchannel, and one without the backchannel.

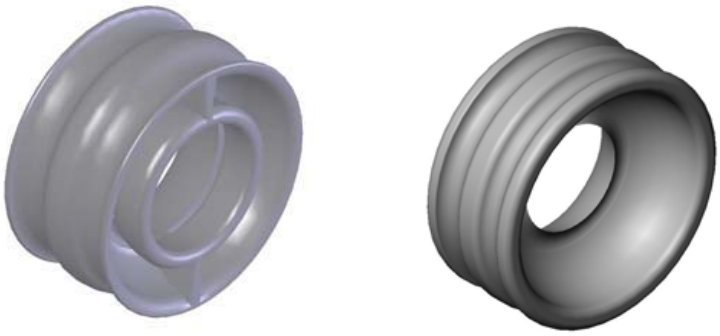

Figure 1.4: Solidworks models of (a) a diode valve with an enclosed backchannel (backchannel diode); (b) diode valve with an open backchannel (open cusped diode) (Camp, 2009).

Several variations of both the backchannel and open cusp diodes were produced, varying both β and α.

The diodes were tested *in vitro* in a mock pulmonary circulatory system (MPCS) and compared based on regurgitate fractions and transvalvular gradients. One design was tested *in vivo* in a pig. The *in vitro* results indicated acceptable levels of regurgitate fraction and pressure gradients for normal levels of PVR. The results of the diode tested *in vivo* were consistent in both tendency and magnitude with the *in vitro* findings (Camp, 2009).

Both *in vitro* and *in vivo* testing of fluid diodes are necessary for the development of new heart valves. *In vitro* testing requires a system that closely mimics the conditions found in a patient. Many mock systems have been developed to study heart valves, but the system of Camp (2009) will be presented here as it was the baseline for the MPCS in this study. Figure 1.5 shows a schematic of Camp's system.

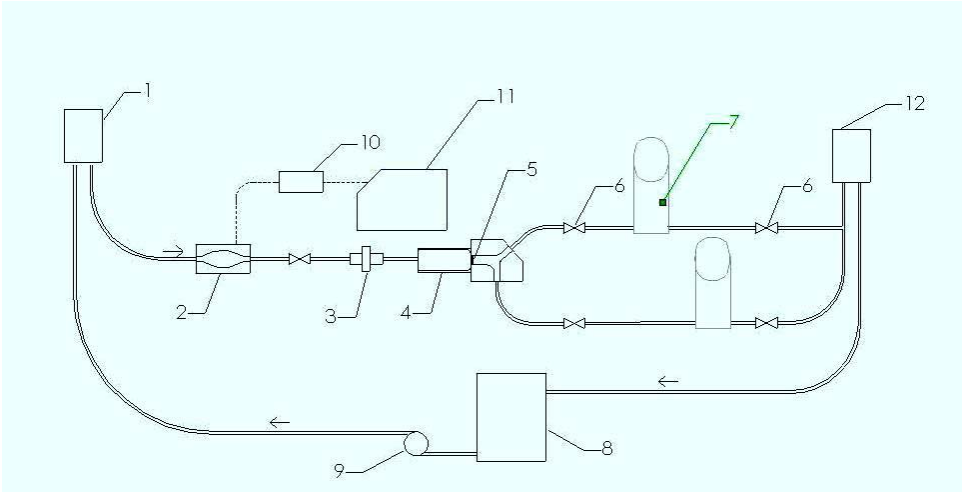

Figure 1.5: Schematic of the mock circulatory system. Arrows indicate flow direction. 1. Right atrium constant head tank; 2. Right ventricular chamber; 3. Flow meter; 4. Test section 5; Mechanical heart valve; 6. Ball valves; 7. Capacitance chambers; 8. Holding tank; 9. Recirculating pump; 10. Pneumatic cylinder; 11. Harvard Pulsatile pump; 12. Left atrium constant head tank (Camp, 2009)

The blood analog starts in a constant-head tank, which models the right atrium, and flows into the right ventricle. The ventricle consists of a balloon enclosed in a chamber. The chamber is cyclically pressurized by a pneumatic cylinder driven by a cam-driven pump (Harvard 1423 Pulsatile pump). The pump is adjustable, allowing the manipulation of heart rate, stroke volume and systolic ratio. The analog then flows through the test section, which is made of acrylic and houses the test valve. A contraction reduces the diameter from 62 mm to 25 mm, which is the size of the prototype valves being studied. The distal section models the human pulmonary artery. Ball valves and windkessel chambers located downstream of the artery provide adjustable resistance and compliance elements respectively. The left atrium is another constant-head tank and is also used to adjust resistance. After flowing through the test section and into the left atrium, the analog drains into a holding tank where it is then pumped up into the right

atrium. This system has one flow probe, located upstream of the valve, and two pressure taps, located just on either side of the pulmonary valve. These allow for instantaneous pressure and flow measurements to be made, but do not allow for ventricular volume calculations. In this study, the ventricle is modified both to improve the ventricular signal and to reduce flow inertance.

A stenotic or incompetent pulmonary valve causes the ventricle to have to work much harder to produce a healthy cardiac output. Fluid diodes have been studied based on their ability to regulate regurgitant fraction and transvalvular pressure gradients, which directly impact the work load on the ventricle. This study is the first to assess the ventricular work load of fluid diodes. Ventricular response is characterized by a pressure-volume loop, or PVL. According to the Frank Starling Law, the heart responds to a change in venous return pressure by adjusting its stroke volume such that the end-systolic volume satisfies the end-systolic pressure-volume relationship (ESPVR). Therefore, by systematically altering the venous pressure for sequential heart beats, a family of pressure-volume loops can be obtained to characterize this response. As illustrated in Figure 1.6, these PVLs define two characteristic curves, the end-systolic pressure-volume relationship (ESPVR) and the end-diastolic pressure-volume relationship (EDPVR) (Burkhoff et al., 2005).

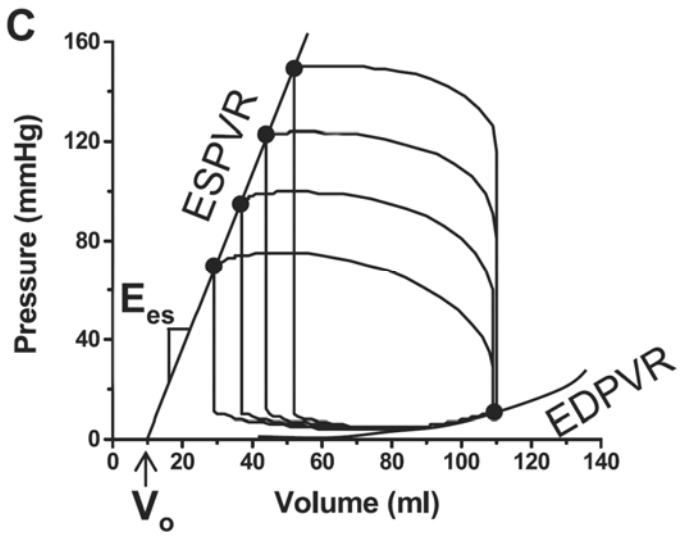

Figure 1.6: Family of PVLs and resulting characteristic curves produced by reducing ventricular preload (Burkhoff, 2005).

Traditionally, it had been difficult to obtain instantaneous volume measurements, making progress in these studies slow. Over the last few decades, however, techniques and devices have been developed to make volume measurements. McKay et al. (1984) investigated the use of impedance catheters to measure volume. This technique was successful in measuring changes in stroke volume, but could not indicate absolute volume measurements. Kass et al. (1986) used conductance catheters to successfully measure ventricle volume and produced clinical PVLs for anesthetized dogs. Unfortunately, conductance catheters are quite invasive and therefore not ideal for use in human patients. Very recently, Baker (2011) has acquired pressure-volume measurements in human patients. A resulting family of PVLs is shown in Figure 1.7.

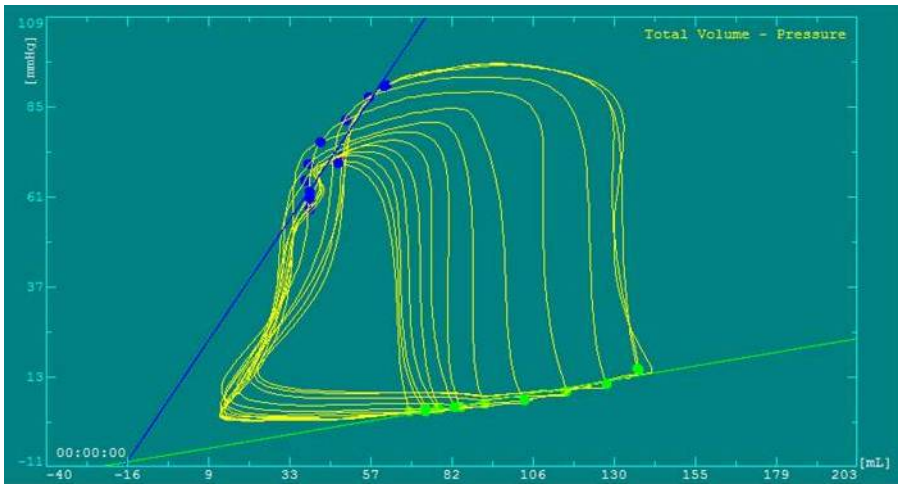

Figure 1.7: Pressure-volume loops obtained clinically (Baker, 2011)

The ESPVR and EDPVR are the result of a natural ventricle adjusting its stroke volume in response to a change in ventricular preload or afterload. The area contained in the PVL is equivalent to the external work per beat (Westerhof et al., 2005). The product of ventricular pressure and flow yields external power, or work per unit time. External energy is found by integrating the power over a heart cycle. Dividing this energy by the period of a heart cycle yields average power.

Scope of this Study

(1) Previous studies at Clemson University have measured pressure and flow during diode testing, and particle image velocimetry (PIV) analysis has been done in the pulmonary artery test section just downstream of the diode (Camp, 2009). However, no clear picture of what exactly takes place within the diode has been presented. Therefore a specific aim of this study is to conduct a two-dimensional flow visualization study of various diode geometries under pulsatile flow conditions. (2) The second specific aim of

this study is to study three diode designs *in vitro* and compare them to a comparable stenosis and also a blank annulus. It is the hypothesis of this study that PVLs produced from *in vitro* testing of various diodes will clearly illustrate a significant reduction in ventricular work as compared to a stenosed or absent valve case. And so the original ventricle is redesigned to accommodate collection of pressure-volume data, and PVLs for the various valve scenarios are obtained for various physiological conditions.

CHAPTER TWO

FLOW VISUALIZATION TEST SECTION AND METHODS

In theory, the diode reduces retrograde flow by redirecting flow and creating a *vena contracta*. It was of interest to see exactly how the diode works in practice; therefore a flow visualization was conducted on several two-dimensional diodes of slightly varying geometries. The flow visualization allowed the effects of the diodes during both systole and diastole to be observed. The two-dimensional test system simply provides a pulsatile flow condition similar to that experienced by a native pulmonary valve, while also providing optical access.

2-D Diodes

The diode shapes used in the flow visualization were produced in SolidWorks by extruding a section view of an existing diode design and then machined from Delrin. These diodes are defined by the dimensions shown in Figure 2.1.

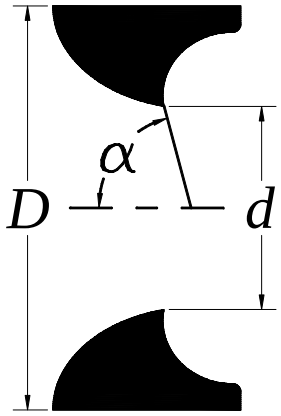

Figure 2.1: Generically dimensioned diode for 2-D testing.

In Figure 2.1, *D* is the outer diameter, *d* is the inner diameter at the cusp, and α is the angle of impingement. α is defined as the angle between the centerline of the diode and a line that could be drawn from the centerline and tangent to the ellipse of the cusp, at the very tip. The value *d*/*D* is the beta ratio, β. The three diodes produced for this study are shown in Figure 2.2. All three have a beta ratio of 0.5, but the angle α varies as 60°, 75° and 90° from left to right. A fourth geometry was tested by placing a vertical glass rod in the center of each open cusp to form a backchannel in the 75° diode.

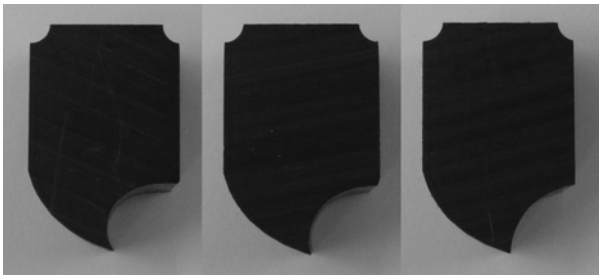

Figure 2.2: Examples of one side of the 2-D diodes with varying angles of impingement.

2-D Test Section

A 2-D test section was used in this study to visually observe the effects of the fluid diodes in a pulsatile flow environment similar to the pulmonary circulation. A full lumped parameter model was not necessary for this flow visualization because the emphasis of this portion of the study is concerned with the pulsatility of the pulmonary circulation. Therefore resistance and compliance elements were not included. The test section (seen in Figure 2.3) was machined from a 24”x8”x1” piece of Delrin, and fashioned so that the diodes could be easily interchanged. A clear acrylic sheet was

bolted on the top and bottom of the test section, forming a sealed chamber. The top sheet was drilled, tapped, and fitted with 1" hose barbs on either end so fluid could be pumped in and out of the chamber. Systolic flow is left to right.

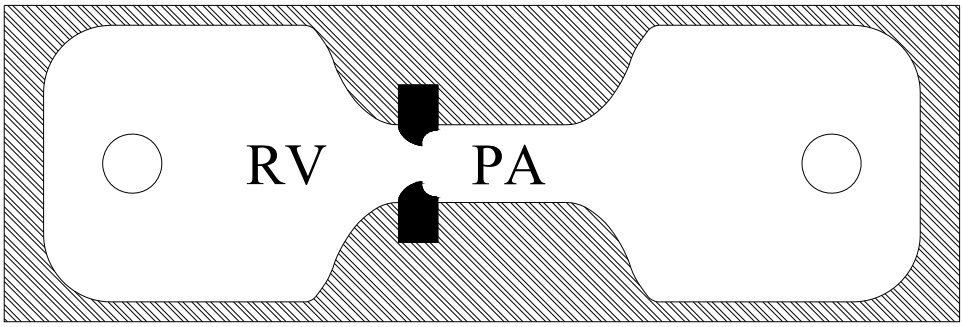

Figure 2.3: 2-D test section and interchangeable diodes used for flow visualization.

The transition from the right ventricle (RV) to the diode was a smooth contour, and on the other side of the diode, a long channel modeled the pulmonary artery (PA). The test setup is shown in Figure 2.4, which shows the pump, test section, and reservoir.

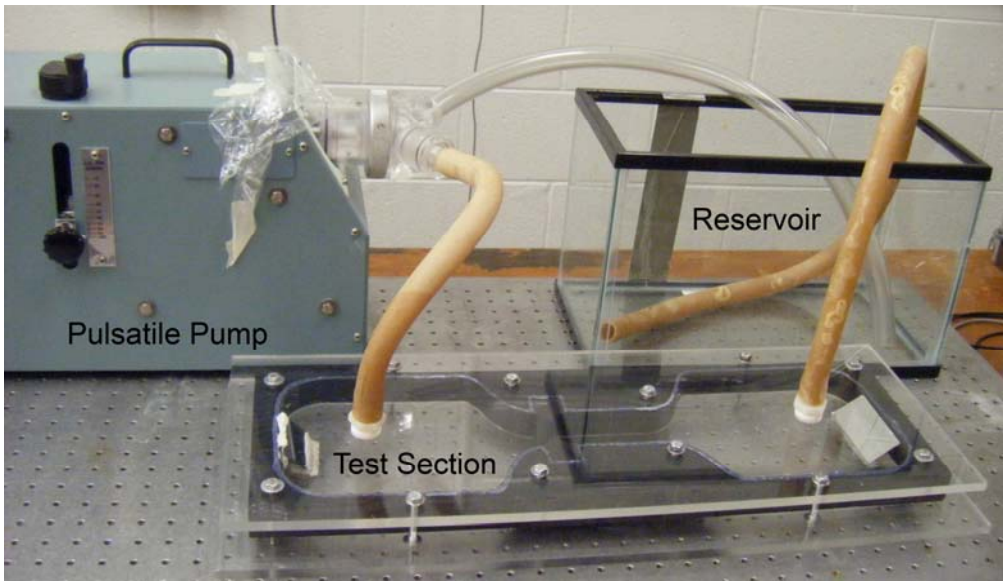

Figure 2.4: 2-D flow visualization test setup (optics and camera not shown).

The flow was driven into the "ventricle" section by a cam driven pump (Harvard 1423 Pulsatile pump) capable of a stroke volume up to 100 cc/stroke and a frequency up to 100 cycles/minute. The output phase ratio of systole to diastole also is adjustable within the pump. During diastole, the pump fills with fluid from both the test section and the reservoir, thus creating a pulsatile flow in the test section. Through a series of mirrors and other optics, a laser sheet was brought into the test section from each side of the test section. This illuminated the 50μm polyamid seeding particles (PSP) within a thin layer of the fluid through the middle of the chamber. The density of the PSP is 1.03 g/cm^3. A Samsung HD digital camcorder was used to record the motion of the illuminated particles at 30 frames/sec. The shutter speed was long enough for the moving illuminated PSP particles to appear as streaks in the individual frames. Each frame was then extracted from the video and observed to determine exactly what occurs during a cycle.

The Stokes number, which is a dimensionless number which characterizes a particle's flow in a fluid, is given by

$$St = \frac{\tau V}{D} \tag{2.1}$$

where τ is the relaxation time, or particle response time; V is the fluid velocity; and D is a characteristic length scale in the fluid flow. The relaxation time is found as

$$\tau = \frac{d_p^2 \rho_p}{18\mu} \tag{2.2}$$

where d_p and ρ_p are the particle diameter and density respectively, and μ is the dynamic viscosity of the fluid. In this flow visualization, with water as the working fluid, a stroke

volume of 100 cc/stroke, and a pulse rate of 70 bpm, the average Stokes number was found to be 0.00106. Since 0.00106 << 1, it can be said that the seeding particles used in the flow visualization do indeed follow the streamlines in the fluid flow, and therefore the streaks in the images illustrate the streamlines in the flow.

Parameter Matching

The purpose of the flow visualization is to observe what effect a fluid diode would have in the place of a pulmonary valve. It is therefore important that the parameters of the tests observed be comparable to those of the human pulmonary circulation system. In this case, the parameters to be matched are those of the mock pulmonary circulatory system (MPCS). In the MPCS, the annulus of the pulmonary artery (PA) has a 25 mm diameter. However, to enhance the flow visualization, the 2-D test section was doubled in size so that the width of the PA was 50 mm. The height remained as 25 mm because that was sufficient to maintain a proper 2-D flow through the middle of the test section where the laser sheet passed through. Due to the increase in size of the test section, the heart rate and stroke volume also had to be increased. A pulsatile flow is defined by two dimensionless parameters: Reynolds number (Re) and Womersley number (α). The Reynolds number is the ratio of inertia forces to viscous forces on a fluid element (Mott, 2006) and is defined as

$$\mathrm{Re} = \frac{VD}{\nu} \tag{2.3}$$

where V is velocity, D is characteristic length (or hydraulic diameter for this study), and ν is kinematic viscosity. The Womersley number, defined in Equation 2.4, describes the pulsatility of a flow and how fully a flow profile can develop between oscillations (Womersley, 1955).

$$\alpha = R\left(\frac{\omega}{\nu}\right)^{\frac{1}{2}} \tag{2.4}$$

In Equation 2.4 $R = \frac{D}{2}$ and is the radius of the blood vessel, ω is frequency, and ν is kinematic viscosity.

Typical Reynolds and Womersley numbers produced for *in vitro* testing in the MPCS are 1314 and 20 respectively. Those are the values while operating the MPCS at a heart rate of 75 bpm and a cardiac output of 5.0 Lpm, and using a blood analogue solution with a kinematic viscosity (ν) of 3.18 mm^2/s. To match these parameters in the 2-D test section for the flow visualization, the required stroke volume and heart rate are 158 cc/stroke and 42 bpm respectively. Unfortunately the available pump is limited to a maximum of 100 cc/stroke. For convenience, flow visualization was conducted for the four diodes simply using water as the working fluid, a heart rate of 70 bpm, and a stroke volume of 100 cc/stoke. While the pulsatile conditions produced in these tests do not perfectly match the conditions found in the MPCS, they are sufficient to demonstrate how the diodes performed under pulsatile conditions. More tests were done with one of the diodes with a blood-analog solution as the working fluid, and the stroke volume and heart rate were varied to determine if the diodes performed similarly over a broad range of

Reynolds and Womersley numbers. The 75° diode was tested with a water-glycerin solution having a kinematic viscosity of 3.20 mm^2/s. The system was operated first with a stroke volume of 100 cc/stroke and a heart rate of 57 bpm. With that setup, the Reynolds number was brought down to 1116 and the Womersley number to 23. These numbers match those of the MPCS within 15%. Then the heart rate was raised to 67 bpm, which brought the Reynolds number to 1312 (a near perfect match) while the Womersley number rose only to 25. These tests were performed to illustrate the validity of the all the flow visualizations done on all the diodes as pertaining to a broad range of pulsatile flows, including the range of Reynolds and Womersley numbers found in the MPCS used for *in vitro* testing of the diodes later in this study.

CHAPTER THREE

IN VITRO TEST SECTION AND METHODS

The flow visualizations in this study explored the effectiveness of the diode design to have a preferential flow direction having lower resistance. Previous literature has indicated that the diode can produce acceptable levels of transvalvular gradients and regurgitant fractions. This study is interested in assessing the diode's ability to reduce the ventricular work load of a heart with a stenosed pulmonary valve. To do so, three diodes of varying geometries were designed and machined to be tested against a stenosis with the same β ratio. Several modifications were made to an existing mock pulmonary circulatory system (MPCS) to create a more physiological environment to test the diodes in, and to allow the collection of total, instantaneous flow into the ventricle. This chapter details the design of the diodes and MPCS as well as the methods for calibration, data collection, and data processing.

Diode Design

Based primarily on previous graduate and undergraduate diode studies conducted at Clemson University, three parametric variations of a fluid diode were designed and produced for assessment in this study. Camp's (2009) results indicated that a beta ratio of 0.5 had a significantly more tolerable TVG than smaller beta ratios. Culbreath (2004) observed that a beta ratio of 0.5 had one of the highest ratios of reverse flow pressure drop to forward flow pressure drops in steady flow studies. Therefore all three of the new

diodes were designed with a beta ratio of 0.5. The entrance nozzle of the diode is prescribed by exactly one quadrant of an ellipse. This ensures a zero angle of impingement for forward flow and thus eliminates any *vena contracta* during systole. The three new designs are show in Figure 3.1. The ellipse that defines the entrance nozzle is the same for all three, but the ellipse that defines the cusp is of varying dimensions so as to accomplish the appropriate angle of impingement.

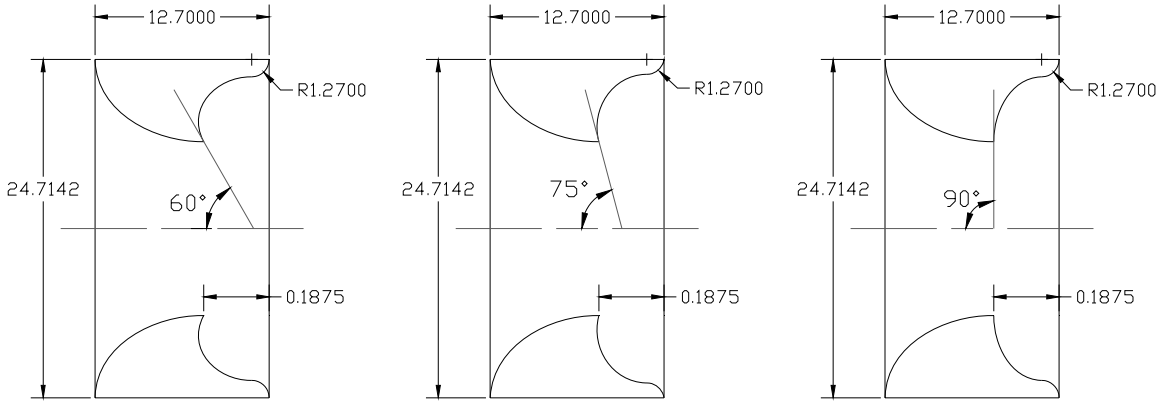

Figure 3.1: Section views of the three new diode designs for current study. Dimensions are in mm; systolic flow is left to right.

The three diodes which were machined from stainless steel to the specifications in Figure 3.1 are pictured in Figure 3.2.

Figure 3.2: Diodes, from left to right: 60°, 75°, and 90°α.

These diodes were tested against a stenosis with similar outer and inner diameters and thickness. The 0.5β stenosis, machined out of delrin is shown in Figure 3.3.

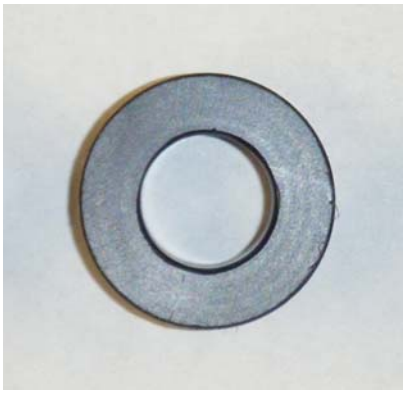

Figure 3.3: A stenosis with 0.5β ratio.

Mock Pulmonary Circulatory System

The *in vitro* testing of the diodes was conducted in a mock pulmonary circulatory system (MPCS). The basis of the system is the lumped parameter network model shown in Figure 3.4. A schematic of the system is shown in Figure 3.5. The values for resistance, inertance, and compliance in Figure 3.4 are listed in Table 3.1.

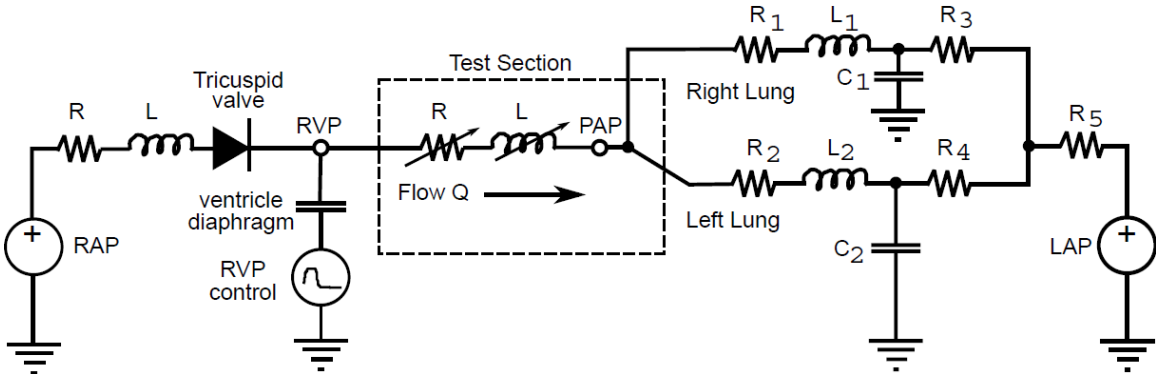

Figure 3.4: Lumped parameter network model for MPCS.

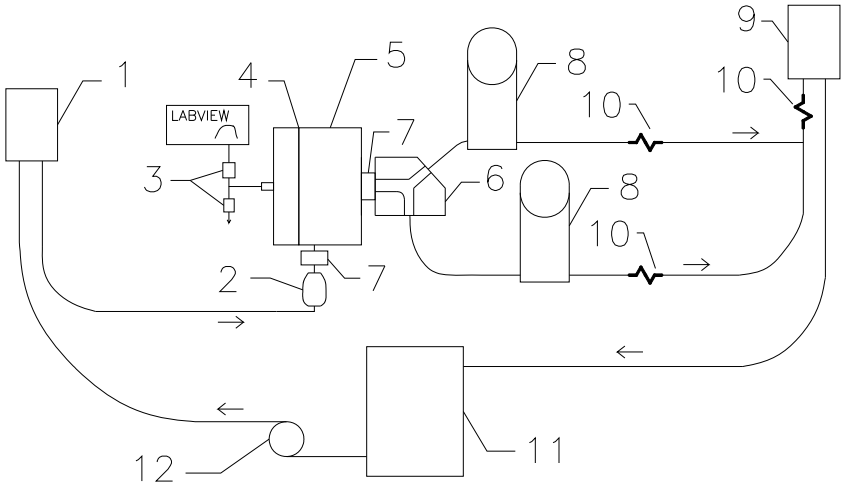

Figure 3.5: Schematic of MPCS used in this study. The arrows indicate flow direction. 1. Upstream head tank; 2. Right atrium; 3. Pressure regulator and vent; 4. Diaphragm; 5. Right ventricle; 6. Pulmonary artery; 7. Flowmeters; 8. Downstream compliance elements; 9. Downstream head tank; 10. Downstream resistance elements; 11. Holding tank; 12. Recirculating pump

Table 3.1: Values for resistance, inertance, and compliance in Figure 3.4

Resistance (mmHg/Lpm)		Inertance (mmHg·s/ml)		Compliance (ml/mmHg)	
R_1	0.120	L_1	0.00367	C_1	1.16
R_2	0.160	L_2	0.00550	C_2	1.16
R_3	0.143				
R_4	0.158				
R_5	0 to 4.5				

In Table 3.1, R_1 and R_2 were measured, R_5 was varied 0 to approximately 4.5 throughout testing, and all other values were calculated.

This system is a modification of a system described by Camp et al. (2007). It contains open air atrial chambers, a programmable, pneumatically driven ventricle, and compliance and resistance elements. It allows for pressure measurements to be obtained in the ventricle and pulmonary artery, and for flow measurements to be obtained from two flow probes, one downstream and one upstream of the ventricle. The flow probe arrangement allows for instantaneous flow measurements and the ability to measure instant stroke volume.

A photograph of the MPCS on the lab table is seen in Figure 3.6. The system is more compact than its predecessor (Camp et al., 2007), reducing both the influence of inertance and the fluid volume used. Further, the pneumatic regulator offers a wider range of heart rate.

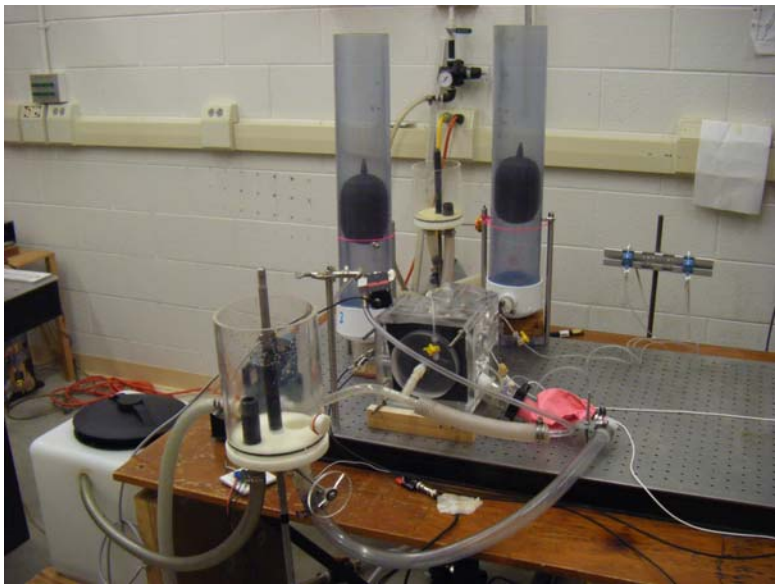

Figure 3.6: Photograph of the MPCS used in this study.

Figure 3.7: Constant-head tank.

The upstream head tank (Figure 3.7) was a 150 mm acrylic tube, closed off on the bottom by a delrin cap. An overflow connection in the tank ensured a constant fluid level, even during the system's pulsatile operation. This tank provided an adjustable constant pressure head for the right atrium.

The original system had a hose connecting the upstream head tank directly to the ventricle. However, to reduce inertance of the fluid upstream of the ventricle, a compliant component was added to function as the right atrium. This was provided by a latex balloon as shown in Figure 3.8.

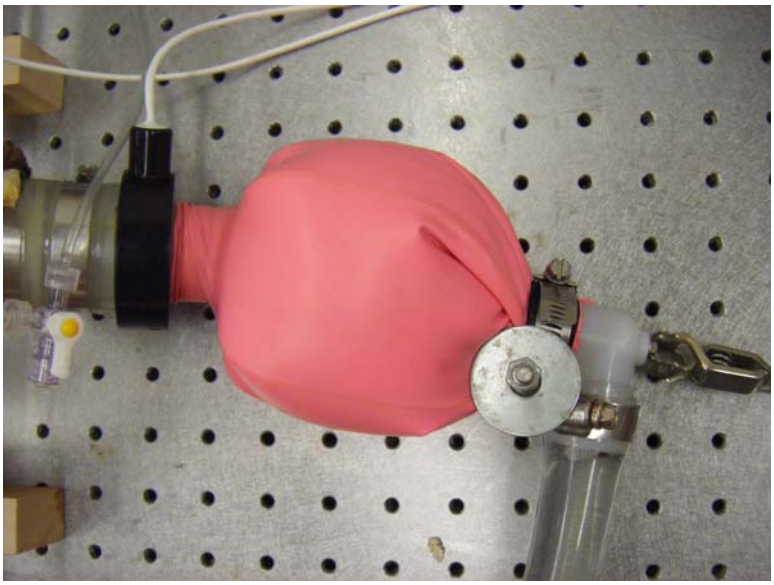

Figure 3.8: Right atrium, which consists of a latex balloon.

Also seen in Figure 3.8 is the upstream flow probe, which monitors the flow through the tricuspid valve. This upstream probe is a Carolina Medical Electronics P6100 electromagnetic flow probe with a 32 mm nominal inside diameter. The tricuspid valve was a SJM bileaflet valve placed in the fitting at the entrance to the ventricle.

The ventricle itself (see Figure 3.9) was a novel design in which power is provided by a pneumatically driven rubber-silicone diaphragm. The ventricle consisted of two chambers bolted together, one for air and one for fluid, separated by this diaphragm. The fluid chamber had a contraction that reduced the ventricle diameter from 127 mm to 25 mm, the size of the diodes tested in this study. The contraction dimensions were similar to those used by previous Clemson researchers, originally taken from a work by Figliola (1976). The contour profile was, however, converted to a series of arcs, for the benefit of the machinist, and scaled up to accommodate the larger dimensions of the new ventricle.

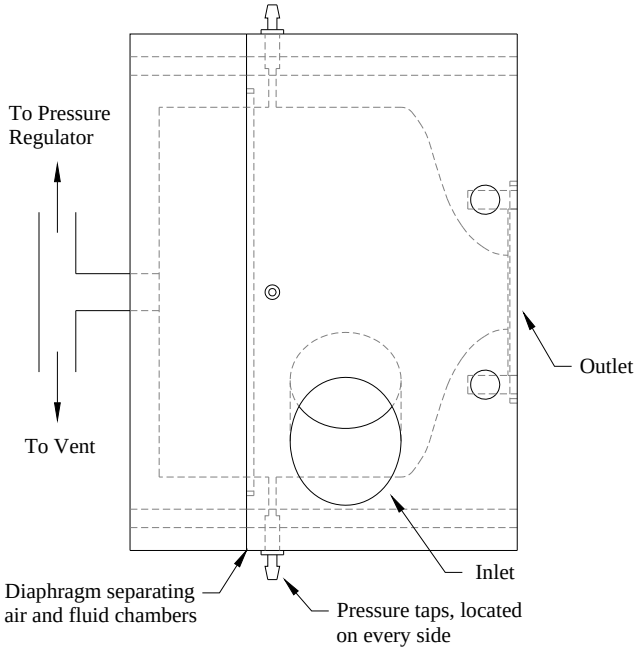

Figure 3.9: Drawing of the right ventricle used in this study.

The fluid chamber of the ventricle was made of clear, polished acrylic. The inlet hole in the fluid chamber was drilled at a 30° angle so that a laser sheet could be brought in through the center of the test section if flow visualization or particle image velocimetry

(PIV) is desired in the future. The downstream side of the ventricle was designed to allow the placement of a flow probe and then tie into the existing pulmonary artery test section used in previous Clemson research.

The pressure wave that drives the diaphragm was shaped by a Hoerbiger variable pressure regulator (Tecno Basic PRE-U series) to create a more physiological systolic signal. While the Hoerbiger provides some venting at the start of diastole, adding an additional 3way flow control valve (MAC, Inc; ISO 3 series) allows the air chamber to vent more quickly, enabling the ventricle to fill properly during diastole. Both the pressure regulator and the vent are controlled by a National Instruments™ LabVIEW™ DAQ system. Figure 3.10 is part of a screenshot from the LabVIEW VI that controls the ventricular drive pressure.

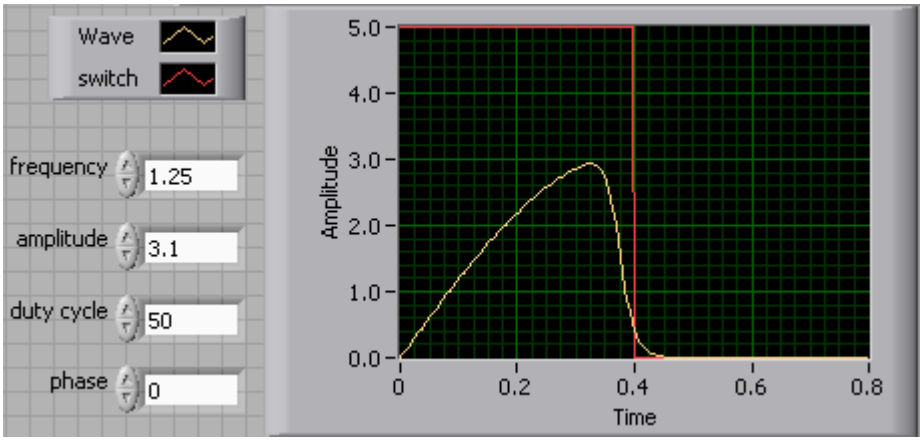

Figure 3.10: Waveform of signal to Hoerbinger and TTL signal to MAC valve.

The waveform sent to the Hoerbinger regulator is labeled “Wave” in Figure 3.10. The following function controls the waveform

$$F(A, f, t) = A\frac{\sin(\pi f t)}{1+\left(\frac{ft}{0.47}\right)^{30}} \tag{3.1}$$

where A is amplitude in volts, f is frequency in Hertz, and t is time in seconds. The function operates very similarly to a simple sine function with an amplitude of A for the first 47% of the cycle. At that point, the term in the denominator rapidly increases in magnitude, driving the function to a near-zero value very quickly. The value of 0.47 was chosen by a trial and error, operating the MPCS with the SJMB valve until the pressure and flow traces indicated a systolic ratio of about 35%. The two parameters of this waveform function which can be changed are frequency and amplitude. The frequency was held at 1.25 Hz throughout the entire study, producing a heart rate of 75 bpm. The amplitude controls the ventricle stroke volume and was adjusted with each MCPS setting so that the cardiac output was maintained at a constant level. The TTL signal, or square wave, in Figure 3.10 controlled the venting MAC valve. The valve would close when the signal was high, and open, or vent, when the signal was low. The two adjustments which could be made to the vent signal were its duty cycle, or duration, and its phase. Both the duty cycle and phase were held constant throughout this study.

The diodes tested fit snugly into the inlet of the pulmonary artery test section. This section was also made of clear, polished acrylic for optical access. The pulmonary artery used (Figure 3.11) is described by Camp (2009). Its only modifications were that the outflow hose barbs were enlarged to reduce resistance. Resistance in the right branch was reduced to 0.12 mmHg/Lpm, and resistance in the left branch was reduced to 0.16 mmHg/Lpm.

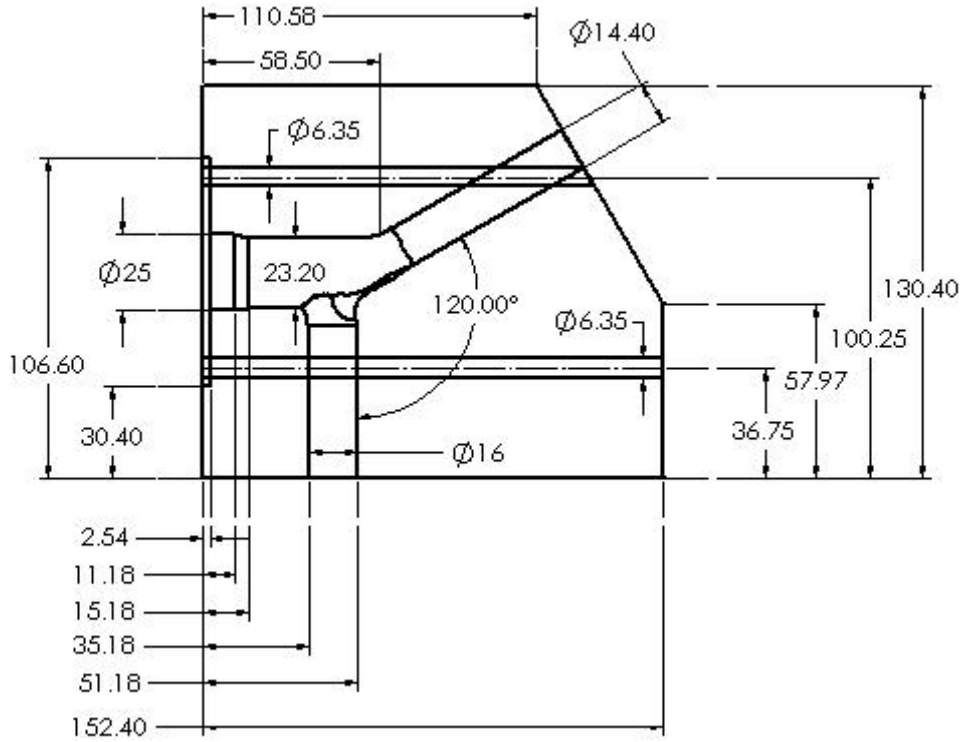

Figure 3.11: Pulmonary artery test section used in this study. Dimension in mm.

Vascular compliance in the system was provided by two Windkessel chambers (Figure 3.12). These were constructed from 100 mm diameter PVC pipes and were 600 mm tall. The bottom ends were capped and had hose barb fittings installed. The top ends are sealed with pneumatic plumber plugs which can be placed at any height in the chamber. As the pressures in the system rises during systole, the air in these chambers gets compressed, and the volume is reduced. This change in volume in response to a change in pressure provides a compliance element for the system. Adjusting the height of the plugs varies the initial volume of trapped air in the chamber and thus provides a means of adjusting the system compliance.

Figure 3.12: Windkessel chamber.

Vascular resistance is added to the system by means of a squeeze clamp on the tubing downstream of the Windkessel chambers (Figure 3.13). There were also ball valves immediately downstream of the Windkessel chambers that were used to balance the flow between the two artery branches. These valves were not used to regulate vascular resistance due to their non-linearity and the imprecision to provide for systematic, minute adjustment. While the squeeze clamp used in this study was also non-linear, it was preferable to the ball valves because the distance between the top and bottom of the clamp could be measured with a caliper, and therefore resistance settings could be systematically replicated from one experiment to the next. The actual resistance of the squeeze clamp was not measured or set for data collection, but rather the clamp was adjusted iteratively until the desired pulmonary vascular resistance (PVR) was achieved. PVR was determined by processing the data after each set was collected.

The constant-head tank downstream of the resistance element modeled the left atrium. It was constructed exactly like the one for the right atrium and could be raised and lowered to set the left atrium pressure at the desired level.

Figure 3.13: Hose clamp used as a resistance element.

Flow exiting the left atrium through the overflow pipe drained into the holding tank where the centrifugal pump could then pump it back up into the right atrium.

Flow, Pressure, and Volume Measurements

The hemodynamics of the MPCS are characterized by the pressures and flows in the ventricle and artery test sections during a heart cycle. The work load on the ventricle is characterized by the instantaneous ventricular volume and pressure during a heart cycle. Measuring both ventricle and arterial pressures and flow both upstream and downstream of the ventricle provided all the necessary information to parametrically evaluate the diodes in this study. All data was acquired using a National Instruments™

automated data acquisition (DAQ) system (NI PCI-6052E card and SCB-68 connection box) and 2008 LabVIEW™8.5 software. Post-processing of data was done using MATLAB®.

Instantaneous and mean flow data immediately upstream and downstream of the ventricle were measured using two flow probes (Carolina Med., P680 and P6100 series) (shown in Figure 3.14) and two Carolina Medical model 501 electromagnetic flowmeter boxes (shown in Figure 3.15).

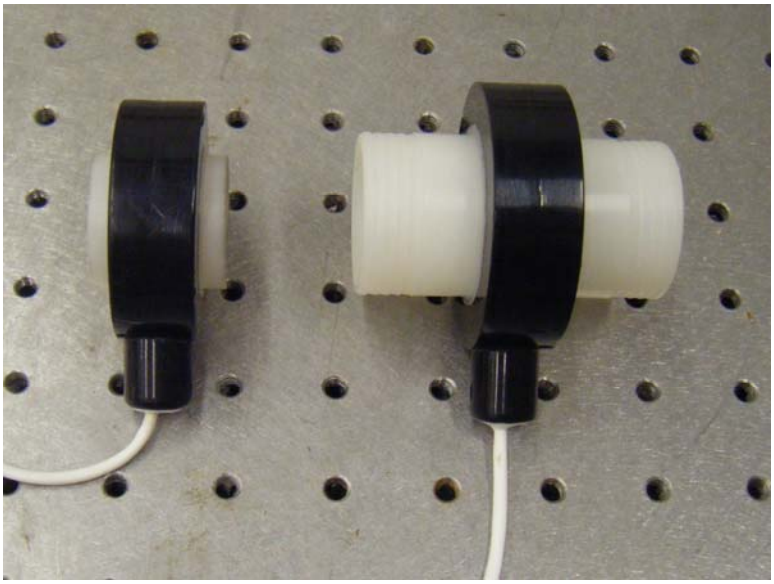

Figure 3.14: EP680 and EP6100 electromagnetic flow probes.

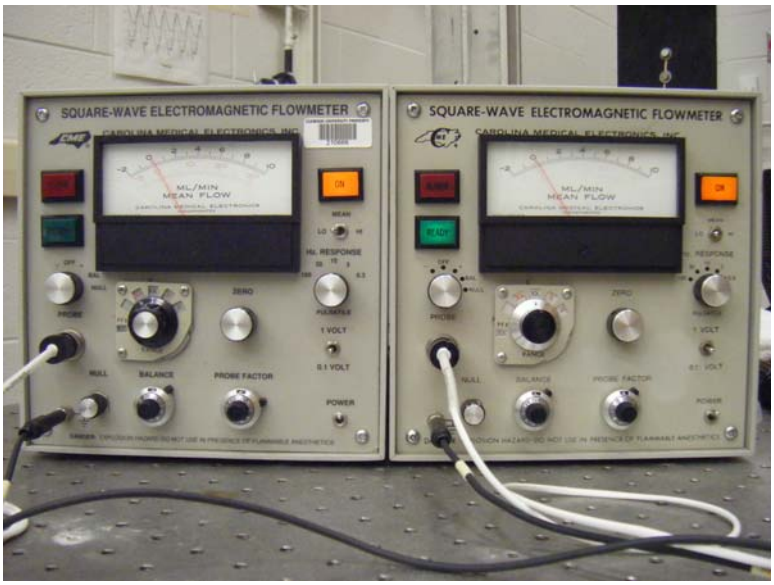

Figure 3.15: FM501 electromagnetic flow meter boxes.

To eliminate signal noise and interference between the two probes, the boxes were connected to each other with a synchronization cable. This ensured that the probes operated in phase with each other. The boxes also shared a common system ground, a stainless steel wire inserted into the ventricle through a spare pressure tap. The flow probes were calibrated using a catch and weigh technique. Sources of error and assessment of the uncertainty in the flow measurements are discussed in the Appendix. Each flow meter box was also zeroed and balanced before each set of tests. During post-processing of the downstream flow data, a zero crossing algorithm used by previous Clemson researchers separated the instantaneous flow data into forward (positive values) and reverse (negative values) flow data. The net forward and reverse flow rates were then determined by time-averaged numerical integration as

$$Q = \frac{1}{\Delta t}\sum_{i=1}^{n} \frac{(Q_i + Q_{i+1}) \cdot (t_{i+1} - t_i)}{2}. \tag{3.2}$$

Equation 3.2 was applied to both the forward and reverse flow rates so that the average forward and reverse flow rates over the whole heart cycle were available. Clinically the regurgitant fraction is calculated as regurgitant volume over the stroke volume. Since $Q_{reverse}$ and $Q_{forward}$ are the average flow rates over the whole cycle, they supplement the regurgitant volume and stroke volume respectively to produce the following equation.

$$RF[\%] = \frac{Q_{reverse}}{Q_{forward}} \cdot 100. \tag{3.3}$$

Right ventricular pressure (RVP) and pulmonary artery pressure (PAP) were measured with BD DTXPlus physiological pressure transducers. Pressure taps were located in the vertical center of both the ventricle and pulmonary artery. The pressure tap on the ventricle was a wall tap, simply a hole drilled in the side with a hose barb to connect a tube from the tap to the pressure transducer. The pressure tap in the artery was a small hole in the side of a catheter tube run through a fitting downstream, up through one of the artery branches to the middle of the artery just downstream of the annulus. Both locations are shown in Figure 3.16. The transducers themselves were located on a stand fixed to the floor rather than the table in order to minimize noise from system vibrations (Figure 3.17) and set at the elevation of the center of the test section to define system zero.

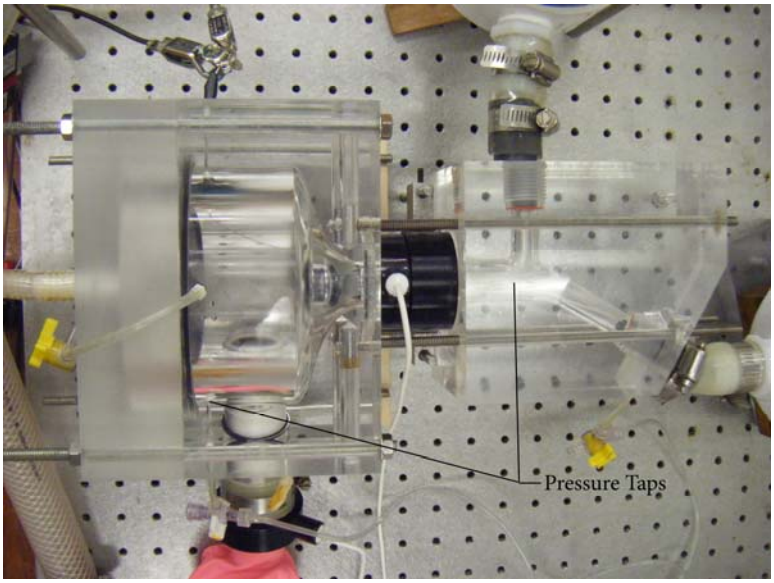

Figure 3.16: Pressure tap locations in ventricle and artery.

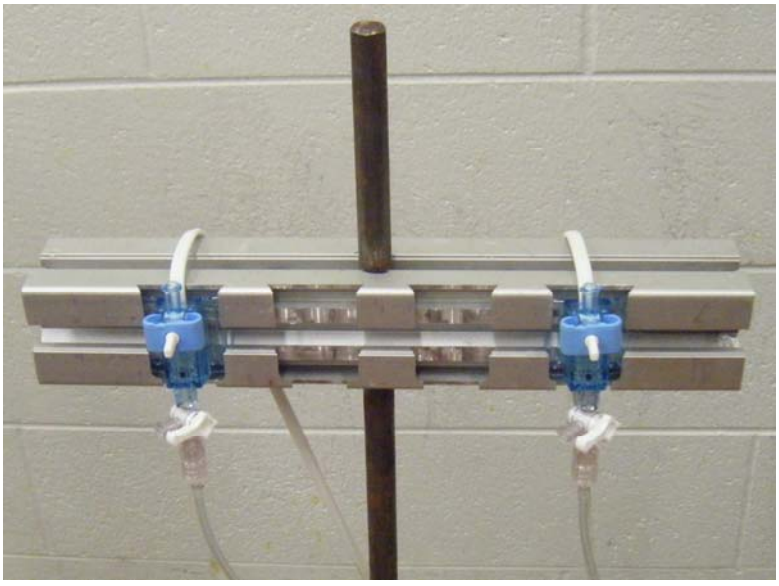

Figure 3.17: BD pressure transducers on isolated stand, at system zero.

The instantaneous transvalvular pressure gradient (TVG) was found as

$$TVG[mmHg] = RVP_{peak} - PAP_{peak}. \tag{3.4}$$

Pulmonary vascular resistance (PVR) and pulmonary vascular compliance (PVC) were derived from the system impedance spectrum as defined by

$$Z(\omega) = \frac{|PAP(\omega)|}{|Q(\omega)|} \tag{3.5}$$

where $|PAP(\omega)|$ and $|Q(\omega)|$ are the pressure and flow spectrums obtained by a Fourier analysis. The zeroth harmonic (Z_0) of the impedance modulus defines the PVR of the system. The PVC of the system is determined by the inverse of the first harmonic (Z_1) of the impedance modulus. The impedance phase can be useful for describing the compliance and inertance of the system as well.

The upstream and downstream instantaneous flow rates provided the measure of the instantaneous volume. The upstream and downstream flow rates were added together with flow into the ventricle considered positive. Then starting with an arbitrary initial volume, the instantaneous volume over one cycle was found by simple backward integration of the total flow into the ventricle as

$$V_{(i)} = V_{(i-1)} + \frac{(Q_{total(i-1)} + Q_{total(i)})\Delta t}{2} \tag{3.6}$$

where $V_{(i)}$ is the instantaneous ventricular volume at a particular timestep i, and Q_{total} is the total flow into the ventricle. Values for V and Q_{total} evaluated at the previous timestep are denoted by subscript (i-1).

Ventricular Work

Ventricular work, energy, and power is determined from the instantaneous ventricular pressure and volume measurements. The external work (*W*), or energy production of the ventricle is defined by the integral of instantaneous power, which is the product of the instantaneous pressure (*P(t)*) and flow (*Q(t)*)

$$W = \int P(t) \cdot Q(t) \cdot dt \,. \tag{3.7}$$

It is important to note that *Q(t)* in Equation 3.7 and 3.8 is the total instantaneous flow of fluid into the ventricle, which is found by combining the upstream and downstream flow signals. Since volume is the integral of instantaneous flow, the external ventricular work can be visualized by the pressure-volume loop (PVL) and is defined by the area enclosed by the PVL. The average power over a heart beat is found by multiplying the work by the heart rate frequency, or with T as the heart period, by

$$P = (1/T) \cdot \int P(t) \cdot Q(t) \cdot dt \,. \tag{3.8}$$

Test Fluids

A nominal 40% by volume glycerin/water solution at 22°C was used for all *in vitro* testing in the MPCS. A small amount of sodium chloride (~1 cc/L) was added to create an electrolytic solution, which is necessary for the electromagnetic flow meters to function properly. The kinematic viscosity of the blood analogue solution, which was checked with a Cannon-Fiske U-tube viscometer, was maintained at about 3.25 cSt.

CHAPTER FOUR

RESULTS AND DISCUSSION

Flow Visualization Results

A parametric flow visualization study was conducted for all four diodes with plain water, a heart rate of 70 bpm, and a stroke volume of 100 cc/stroke, as previously discussed in Chapter Two. The 75° diode was also then tested under various pulsatile conditions closely matching those found in the mock pulmonary circulatory system (MPCS), based on Reynolds Number (Re) and Womersley Number (α), so that conclusions could be made of the diodes' performance over a broad range of pulsatile conditions.

Systolic Performance

Figure 4.1 shows peak systolic flow photographs for each diode design tested. The direction of the flow in each image in Figure 4.1 is from left to right. In the figure, the pictures from left to right are for diodes having apex angles of 60^o, 75^o, 75^o with backchannel, and 90^o, respectively.

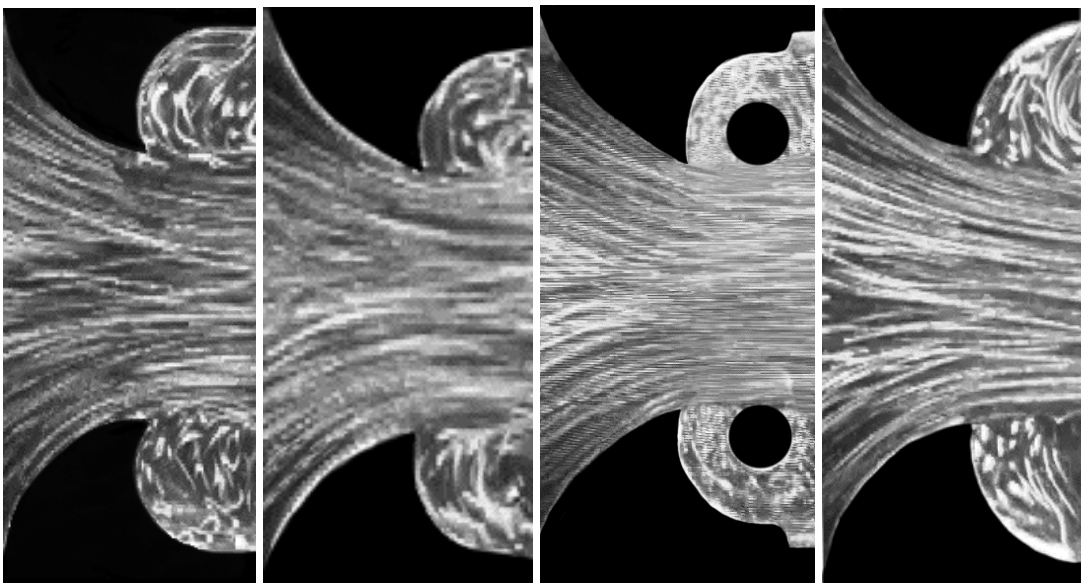

Figure 4.1: Function of all four diodes during systole. From left to right: 60^o, 75^o, 75^o with backchannel, and 90^o diodes. Photo duration is 33.3 ms.

In the tests in which the photographs in Figure 4.1 were taken, the working fluid is water (ν=0.9634 mm^2/s), the stroke volume is 100 cc/stoke, and the heart rate is 70 bpm, which results in an average Reynolds number of 3178 and a Womersley number of 46.7 in the pulmonary artery of the 2-D test section. The photographs taken during peak systole indicate that the diode designs function almost identically to each other during systole. Each photograph in Figure 4.1 reveals a strong jet through the nozzle entrance with a little vortex forming inside the cusp on both sides of the diode. The jet fills the entire width of the diode between the two cusps, and there is no significant flow separation through the nozzle up to the cusps. Therefore during systole, the antegrade flow is funneled through the diode and can flow through the entire 25.4mm cross-section. The similarity of flow in systole between the diode designs is not unexpected given the identical inflow nozzle profile used for each. One of the concerns with the diode design

was the possibility for the cusps to produce a small area where blood could stagnate and promote thrombosis. However, the vortices seen in the photographs in Figure 4.1 effectively "flushed out" the cusps continually during systole so that there were no stagnant areas. The vortices move downstream as illustrated in the sequence of images in Figure 4.2 and eventually dissipated. Direction of the flow in Figure 4.2 is left to right.

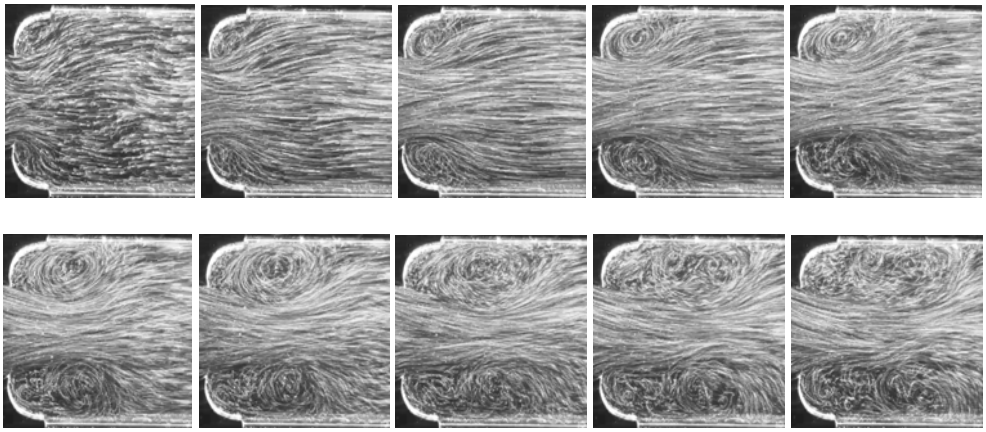

Figure 4.2: Sequence of images during systole immediately downstream of the cusp of the 75° diode. Photo duration is 33.3 ms for each image.

Diastolic Performance

Figure 4.3 shows the photographs for each diode under the aforementioned conditions but during diastole. The direction of the flow in each image in Figure 4.3 is primarily from right to left. In the figure, the photographs from left to right are for diodes having apex angles of 60^o, 75^o, 75^o with backchannel, and 90^o, respectively.

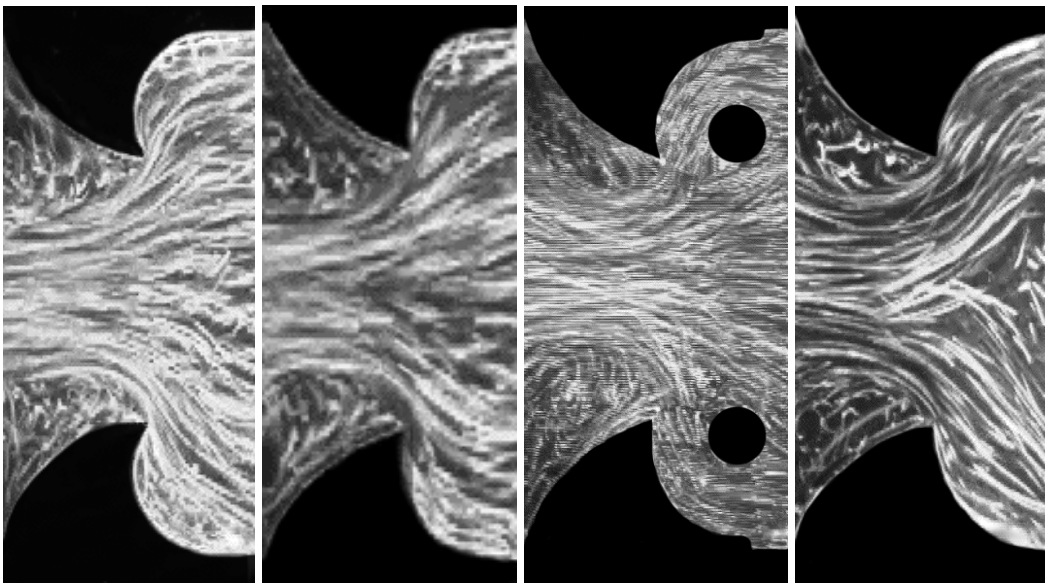

Figure 4.3: Function of all four diodes during diastole. From left to right: 60^o, 75^o, 75^o with backchannel, and 90^o diodes. Photo duration is 33.3 ms.

As seen each photograph in Figure 4.3, there is significant flow separation as the cusp of the diode redirects the flow from the outside of the artery towards the center of the diode. This results in a *vena contracta* that effectively reduces the area that the regurgitant flow can pass through. The distance between the two cusps of the each diode is 25.4 mm, but clearly the regurgitant flow can only flow through a reduced portion of this cross-section. Each of the photographs in Figure 4.3 was imported into AutoCAD and scaled to the correct size. Then the effective cross-section, which is reduced by the *vena contracta* was easily measured. For the diode with the 60° apex angle, the effective flow area is reduced to 14.9 mm across. For the diode with the 75° apex angle, the effective flow area is reduced to 13.2 mm across. For the diode with the 75° apex angle and a backchannel, the effective flow area is reduced to 14.7 mm across, which, while it is a slight improvement of the 60° diode, it is not an improvement over the 75° diode with no backchannel. For

the diode with the 90° apex angle, the effective flow area is only reduced to 16.7 mm across, which gives it the poorest performance of all four of the designs. The 2-D test section has a depth of 25.4 mm, therefore the 75° diode, which performed the best, reduced the effective area from 654 mm^2 to 335 mm^2, a 48% reduction. It is expected that a diode placed in the MPCS would reduce the effective area during diastole even more since the *vena contracta* will have a three-dimensional effect.

Pulsatile Parameter Matching

The photographs in Figures 4.1 and 4.3 provide a comparable analysis between the varying diode geometries in a pulsatile system; however, the average Reynolds and Womersley numbers under those testing conditions did not perfectly match those found under normal operating conditions in the MPCS where the 3-D diode designs are tested. Therefore the diode with the 75° apex angle, which performed the best in those tests, was tested again under pulsatile conditions that closely matched those found in the MPCS. The purpose of these tests was to determine if the 75° diode performs similarly under a range of Reynolds and Womersley numbers which encompasses those found in the MPCS. The 75° diode was tested with a water-glycerin fluid having a kinematic viscosity comparable to blood (ν=3.20 mm^2/s). The 2-D system was run with a stroke volume of 100 cc/stroke and a heart rate of 57 bpm, yielding a Reynolds number of 1116 and Womersley number of 23. This was the setup that matched both Reynolds and Womersley as close as possible to that of the MPCS, about 15% error for both parameters. The system was then run with the heart rate raised to 67 bpm, which matched

the Reynolds number for the MPCS (1314) but raised the Womersley number to 25. Figure 4.4 below shows the systolic pictures comparing the 75^{o} diode tested in water to those tested in the water-glycerin mixture. From left to right they are the diode in water with a heart rate of 70 bpm, in water-glycerin at 57 bpm, and water-glycerin at 67 bpm. The direction of the flow in each image in Figure 4.4 is from left to right

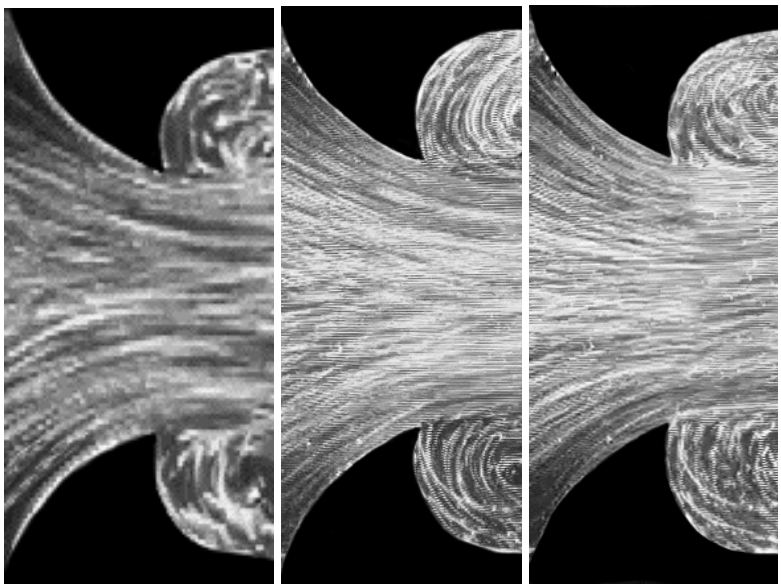

Figure 4.4: Function of the 75° diode during systole, varying working fluid and heart rate. From left to right: the diode in water with a heart rate of 70 bpm, in water-glycerin at 57 bpm, and water-glycerin at 67 bpm. Photo duration is 33.3 ms.

The three photographs in Figure 4.4 are nearly identical to each other, and therefore suggest that the performance of the diode during systole remains the same for the range of Reynolds and Womersley numbers represented by these tests. The results of comparing the three setups during diastole are also very similar. Figure 4.5 below shows the diastolic pictures in the same order as above. The direction of the flow in each image in Figure 4.5 is primarily from right to left.

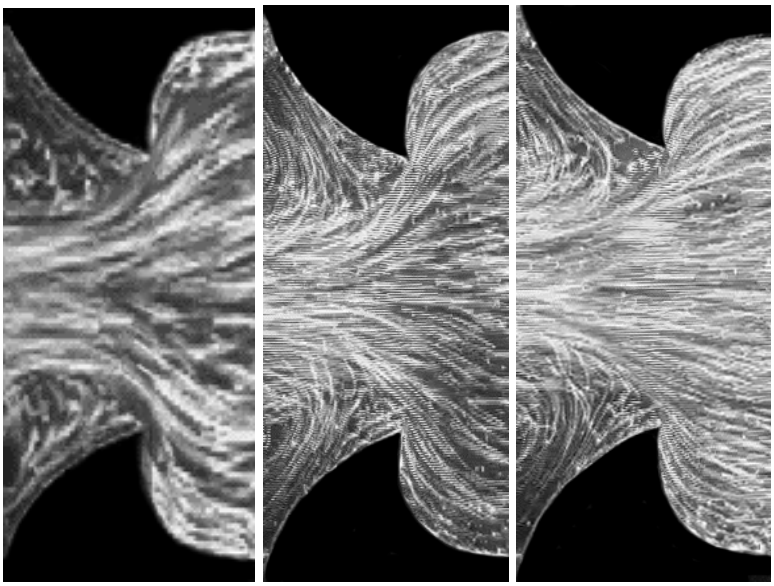

Figure 4.5: Function of the 75° diode during systole, varying working fluid and heart rate. From left to right: the diode in water with a heart rate of 70 bpm, in water-glycerin at 57 bpm, and water-glycerin at 67 bpm. Photo duration is 33.3 ms.

It is clear that the diode has essentially the same effect in each setup. In all three of the photographs in Figure 4.5, the cusps of the diode function similarly by redirecting the retrograde flow towards the center of the diode, creating a *vena contracta*. It is important to notice from this comparison is that the diode performed essentially the same across the range of flows in which it was tested. This confirms that the tests run on the varying diode geometries in plain water are indeed valid indicators as to how the diode will affect regurgitant flow in the MPCS.

The flow visualization clearly shows that all of the diodes tested functioned as they were designed to by reducing the effective area that retrograde flow can pass through. The typical systolic and diastolic patterns created by the diodes are illustrated in the drawings below.

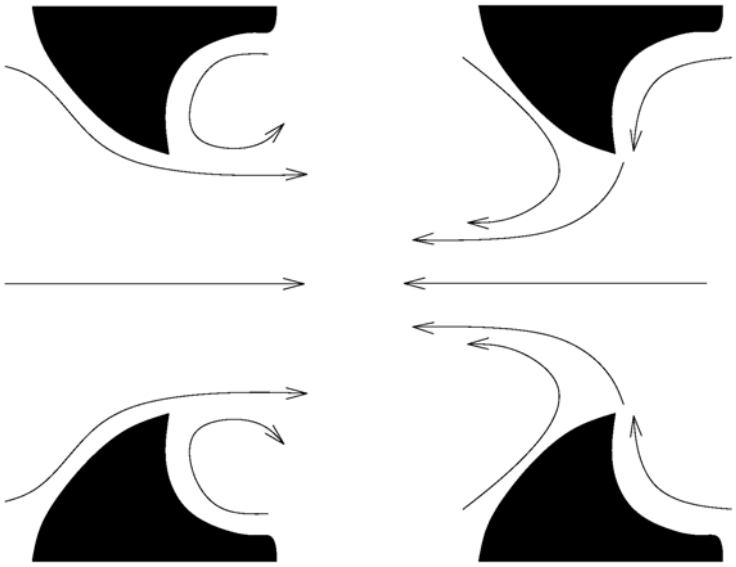

Figure 4.6: Typical systolic (left) and diastolic (right) flow profiles through diode.

The inlet nozzle of each diode funneled the antegrade flow through the diode, creating a strong jet with vortices on either side of it. The vortices, which originate in the cusps at the onset of systole, proceed downstream between the jet and the artery walls until the end of systole. During diastole, the cusp of each diode re-directed the outside flow toward the center of the channel, creating a *vena contracta*. This *vena contracta* reduced the area through which the fluid could flow. The parametric studies done on the diodes with water as the working fluid indicate that the diode with the apex angle of 75^{o} provides the largest flow area reduction with its *vena contracta* during diastole. This suggests that it has the best diastolic performance in reducing regurgitant flow.

MPCS Test Results

A parametric study was conducted with three diode designs, and they were compared to each other as well as to a comparable stenosis and a blank annulus. Tests were run with the diodes placed in the right ventricular outflow tract (RVOT) as well as just downstream of the pulmonary artery annulus. Pressures and flow rates were measured, and device performance was evaluated based on regurgitant fraction, transvalvular gradient, and ventricular work. Parametric variations of the diode design were tested in the MPCS under conditions relevant to human physiology.

Test Conditions

For the parametric *in vitro* testing in the MPCS, the following conditions were maintained: cardiac output between 5.00 and 5.20 Lpm, pulse rate of 75 beats per minute (bpm), and a systolic ratio of about 40%. The pulmonary vascular resistance (PVR) was varied between 1 and 5 mmHg/Lpm, and the pulmonary vascular compliance (PVC) which is coupled with PVR, varied between 2 and 5 ml/mmHg. The PVR was varied by changing the downstream resistance by adjusting the resistance clamp. Cardiac output was maintained by varying the stroke volume of the ventricle. Stroke volume was found to be a function of PVR because as the resistance was increased, RF also increased, and as RF increased, the stroke volume had to be increased to maintain a constant CO.

In this study, the first 25 cycles of each data set were analyzed to determine all of the results. It was of interest to ensure that having N=25 was sufficient for the results to be independent of sample size. Several sets of data, from various valve devices and with

varying PVR, were processed with N=13 and then N=25. The results using the two sample sizes were then compared to each other. In all of the data sets checked, the peak and mean pressures varied less than 0.2%, mean flow (CO) varied less than 0.4%, and the calculated values for PVR, PVC, TVG, RF, and ventricular work varied less than 0.8%. This indicates that N=25 is indeed a sufficient number of cycles for an analysis.

It was also of interest to determine the consistency of the MPCS over time and between data sets, or how well the experiments could be controlled. To gain this insight, the MPCS was run continually, and several sets of data were collected, analyzed, and compared. This was done for multiple valve devices and for various PVRs. Across the board, the results of the repeated experiments were very consistent. Between the consecutively repeated data sets with the same MPCS settings, the pressure measurements typically differed by less than 2%, and flow measurements by less than 3%. The calculated values for PVR, PVC, TVG, RF, and ventricular work in the consecutive data sets varied from set to set by less than their 95% confidence level uncertainties. This indicates that the experiments are well-controlled and that the data and its results do not vary significantly over time.

System Verification

The MPCS was operated using a St. Jude Medical Bileaflet (SJMB) mechanical valve to ensure that physiological behavior of pressures and flow rate could be simulated. Pressure-Volume loops were obtained with the SJMB valve to demonstrate the system's capability to determine ventricular work. The MPCS was operated over a range of PVR,

and the right ventricular pressure (RVP), pulmonary artery pressure (PAP), and flow rate signals upstream (Q_u) and downstream (Q_d) of the ventricle were measured. A typical pressure and flow trace with the SJMB is shown in Figure 4.7. The settings in the MPCS when this trace was obtained were as follows: CO of 5.10 ± 0.130 Lpm (95%), HR of 75 bpm, PVR of 3.26 ± 0.170 mmHg/Lpm (95%), and PVC of 2.51 ± 0.188 ml/mmHg (95%). These pressure traces were generally consistent with physiological traces shown by Rosendorff, (2001) which are shown in Figure 4.8.

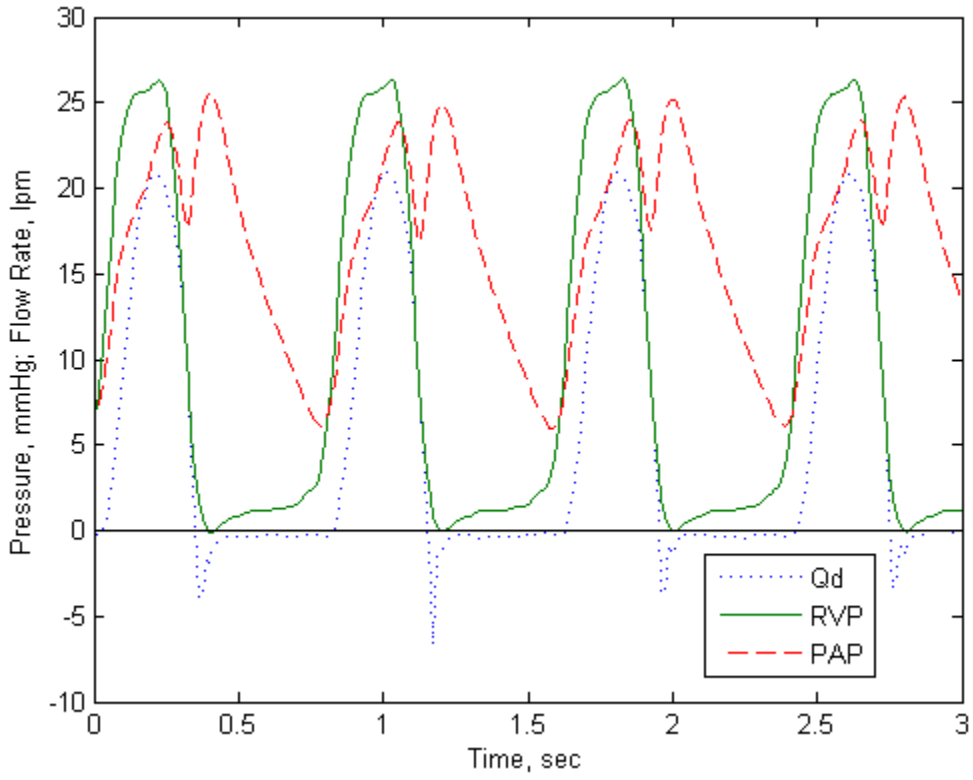

Figure 4.7: Physiological signals for the SJMB valve.

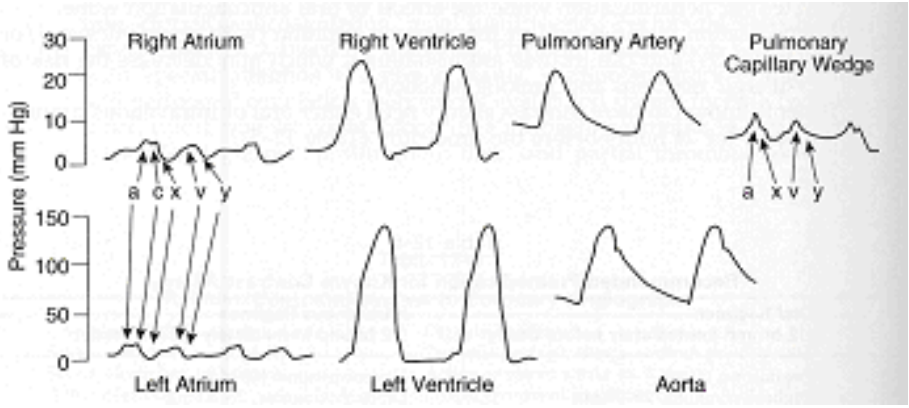

Figure 4.8: Pressure signals in the heart. (Rosendorff, 2001)

During diastole, the flow should be zero. With the SJMB valve however, the trace hovers slightly below zero due to a small amount of valve leakage. At the onset of systole, the ventricle pressure rises sharply. When it overcomes the artery pressure, blood begins to flow downstream through the valve, and the flow trace rises with the ventricle pressure. As the ventricle pressure peaks, so does the flow, and both fall together as diastole begins again. The artery pressure, which also rises during systole, displays a distinct dicrotic notch which occurs as the pulmonary valve closes. This notch coincides with the sharp negative spike in the flow signal which is caused by leakage as the valve closes.

The dicrotic notch in the PAP signal is more accentuated than is generally seen in clinical data, and the wave directly following the notch is unusual. While it can not be proved, this study attributes this wave to pressure waves reflecting through the non-compliant pulmonary artery test section.

Figure 4.9 is a typical pressure and flow trace for the 0.5β stenosis. The settings in the MPCS when this trace was obtained were as follows: CO of 5.13 ± 0.150 Lpm

(95%), HR of 75 bpm, PVR of 2.81 ± 0.168 mmHg/Lpm (95%), and PVC of 2.70 ± 0.0690 ml/mmHg (95%). While the magnitudes of the traces of pressure in Figure 4.9 vary with PVR, the general shape of the signals stay the same; therefore only this one figure is presented. Throughout the stenosis testing, as the PVR was raised, the amplitude of the pressure wave driving the ventricle had to be increased in order to maintain a consistent cardiac output between 5.00 and 5.20 Lpm. As the amplitude of the driving pressure wave was increased, the systolic pressure in the ventricle also increased. As seen in Figure 4.9, even for a PVR of 2.81, which is within the normal range for an adult, the ventricle must produce abnormally high pressures to produce the required output. The transvalvular gradient is also severe, at 34.0 ± 0.910 mmHg.

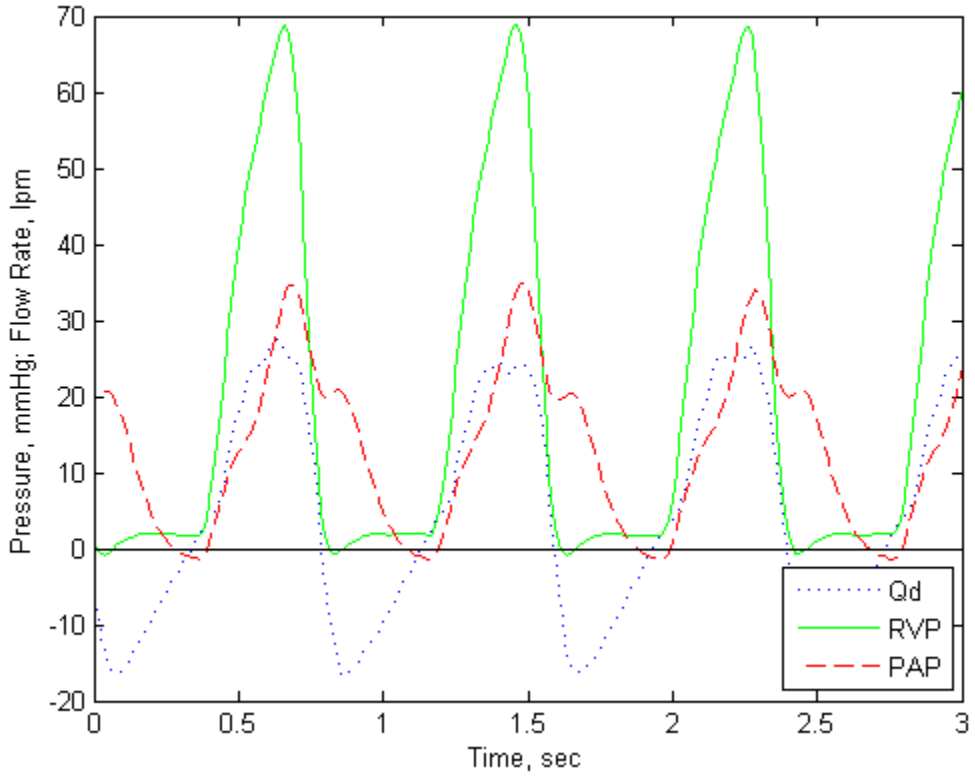

Figure 4.9: Physiological signals for a 0.5β stenosis.

Typical physiological traces for a diode in this MPCS are shown in Figure 4.10. The traces for all three diodes are very similar to each other; therefore just this trace for the 60°α diode is presented. The settings in the MPCS when this trace was obtained were as follows: CO of 5.02 ± 0.210 Lpm (95%), HR of 75 bpm, PVR of 2.78 ± 0.191 mmHg/Lpm (95%), and PVC of 2.53 ± 0.0970 ml/mmHg (95%).

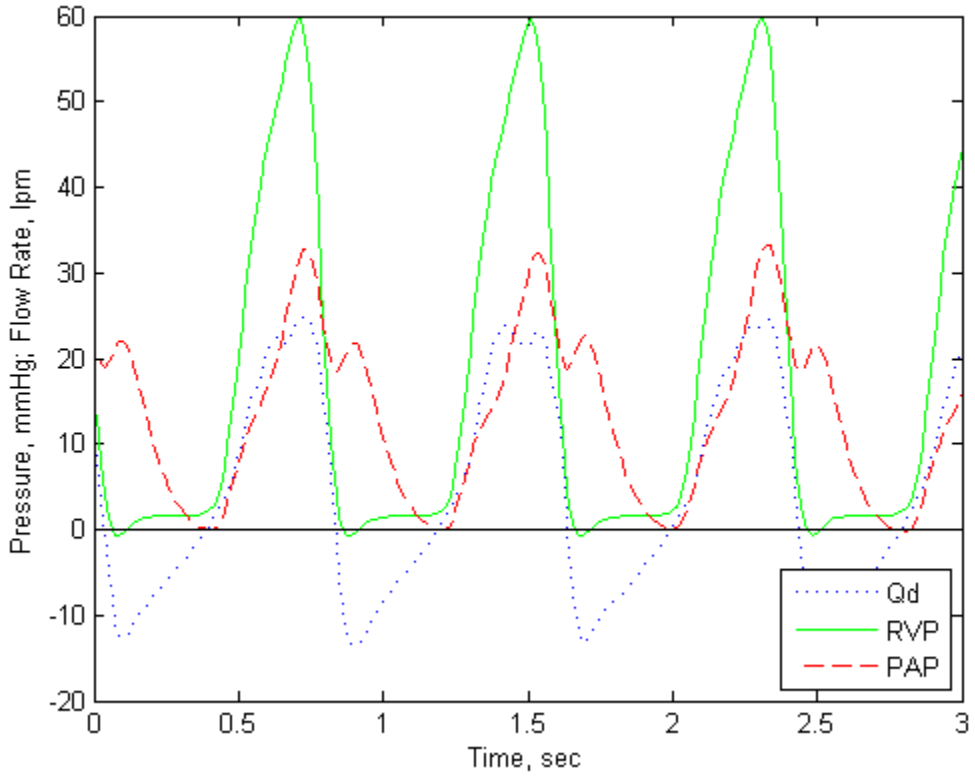

Figure 4.10: Physiological signals for a 60°α diode.

The shapes of the pressure and flow signals are very similar for the stenosis and diodes. As seen in Figure 4.10, the diode also creates a higher than normal peak RVP, but the transvalvular gradient of 27.0 ±1.06 mmHg (95%) is tolerable (Alexander, 1998). Both the peak RVP and TVG for the diode are an improvement over the stenosis.

Fourier Analysis

A Fourier analysis of the input impedance (given by Equation 3.5) was used to determine PVR and PVC for a set of data. Clinically, PVR of a pulmonary system is

determined by the average PAP divided by the cardiac output, or average flow as shown in the following equation.

$$PVR\left[\frac{mmHg}{L/\min}\right] = \frac{PAP_{mean}}{CO} \tag{4.1}$$

The zeroth harmonic of a Fourier transform of a signal is the average of that signal. Therefore, the zeroth harmonic of the impedance modulus gives the value for the average PAP over the average flow and thereby defines the PVR of the system for that data set. Weinberg et al. (2004) observed excellent correlation between clinical measurements of PVR the zeroth harmonic of the impedance modulus. Weinberg also found an inverse relationship between the first harmonic of the impedance modulus and *in vitro* testing of PVC. Clinically, PVC of the pulmonary system is found as

$$PVC\left[\frac{ml}{mmHg}\right] = \frac{CO}{PAP_{pulse} \cdot HR} \cdot 1000 \tag{4.2}$$

where PAP_{pulse} is the pulse pressure, or difference between the maximum and minimum PAP pressures. Camp (2009) calculated PVR and PVC using both the clinical and Fourier analysis methods and found them to be very well correlated. In this study the Fourier analysis method is used to determine PVR and PVC.

The Fourier analysis was done using the FFT (fast Fourier transform) function in Matlab®. Twenty five consecutive cycles of data were analyzed for each data set. The FFT function was applied to the downstream flow and PAP data sets, and the impedance spectra for those twenty five sets were found by dividing the PAP spectra by the flow spectra. An ensemble average was then taken of the twenty five impedance spectra to

produce one impedance spectrum characteristic of the entire data set. The impedance modulus is the magnitude of the spectrum. Figure 4.11 is a typical plot of the impedance modulus for the SJMB valve. The MPCS settings for this data set were as follows: CO of 5.10 ± 0.03 Lpm, HR of 75 bpm, and PVR of 3.26 ± 0.17 mmHg/Lpm. Figure 4.11 was produced by plotting the magnitudes of the harmonics of the impedance spectrum against their corresponding frequencies. The harmonics of the spectrum are found at multiples of the fundamental frequency of the data set, which is 1.25 Hz, corresponding to the heart rate, which was 75 bpm. The impedance phase plot for the same data set is shown in Figure 4.12. This plot was produced by plotting the phase angles of the harmonics of the impedance spectrum against their corresponding frequencies.

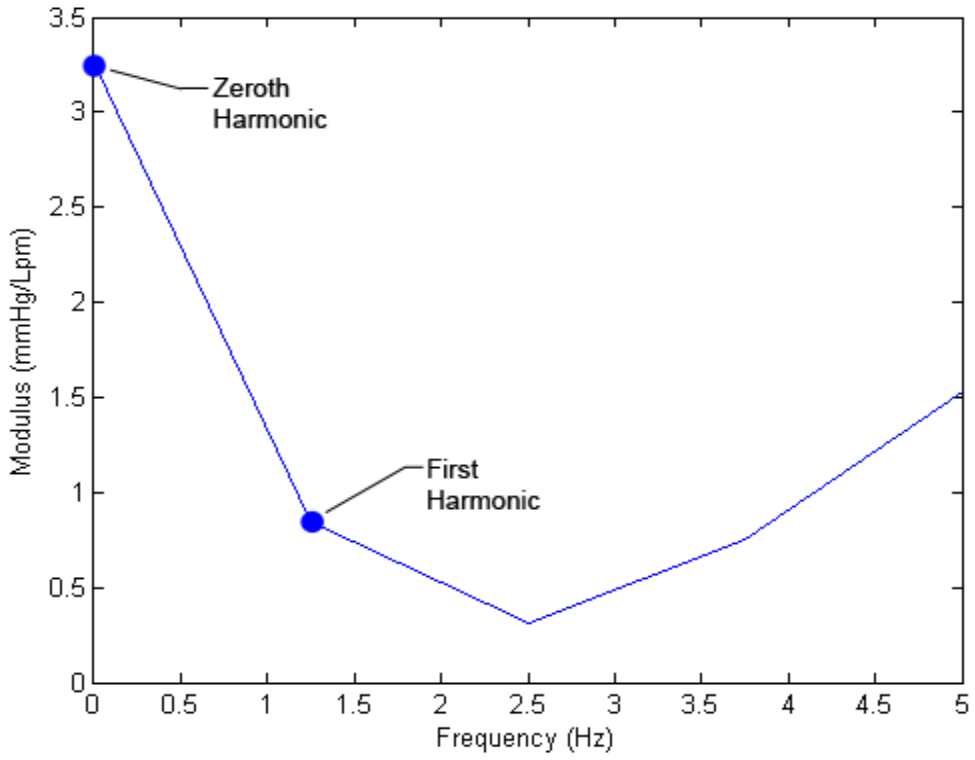

Figure 4.11: Typical impedance modulus plot for the SJMB valve.

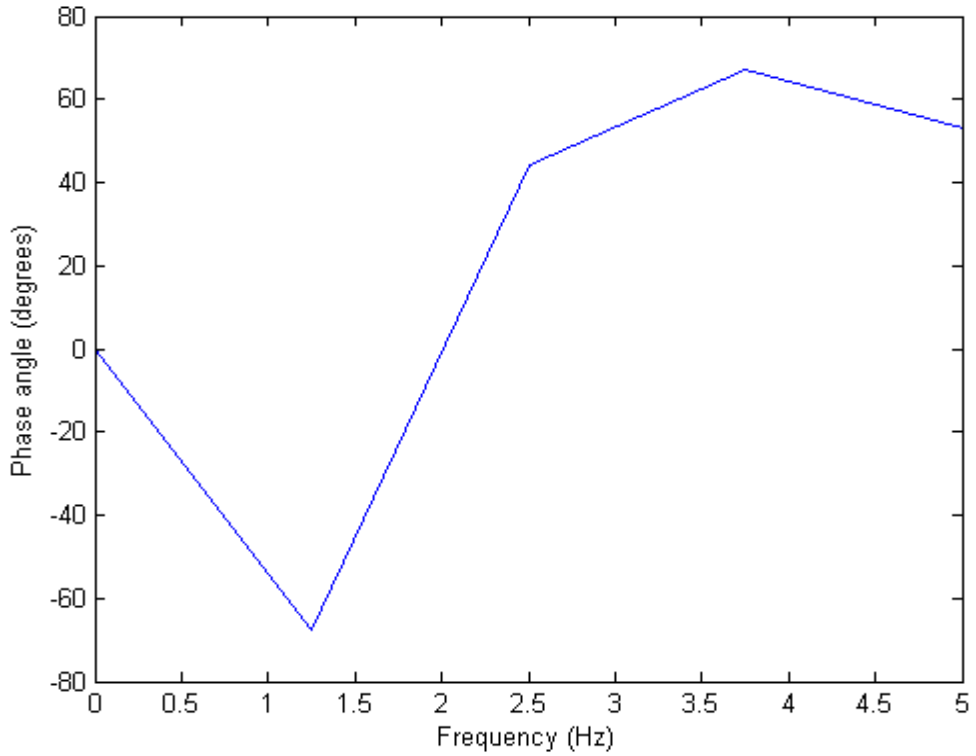

Figure 4.12: Typical impedance phase plot for the SJMB.

In general, both the impedance modulus and phase plots are consistent with those of a natural cardiac system as shown by Westerhof et al., (2005). In Figure 4.11 the zeroth harmonic and inverse of the first harmonic match the PVR and PVC for that data set as determined by Equations 4.1 and 4.2. Typically the amplitudes of the higher frequency harmonics can be averaged to determine the characteristic input impedance. However, due to the 5 Hz filters placed on the pressure data, any component of the impedance spectrum at a frequency higher than 5 Hz has been attenuated and not reliable. The phase plot, which starts at zero degrees and immediately drops to a negative value, indicates that the MPCS is indeed a compliant system.

Ventricular Work

Ventricular work was extracted from a pressure-volume loop analysis of the cardiac cycle. The total flow into the ventricle was found by subtracting the downstream flow through the pulmonary valve (Q_d) from the upstream flow through the tricuspid valve (Q_u). The instantaneous volume of blood in the ventricle was then found by integrating the instantaneous flow of blood into the ventricle. The method of integration used was a discrete backward trapezoidal integration beginning with the second data point in the set.

$$V(t) = V_{(t-1)} + \frac{1}{2}\left(Q_{(t-1)} + Q_{(t)}\right)\Delta t \tag{4.3}$$

The first data point, or the initial volume, was set to 160 ml, which is significantly larger than a typical human end-diastolic volume. However, it was necessary for the initial volume to be so large because in some of the tests with a higher system PVR, the stroke volume required to accomplish the correct cardiac output approached 160 ml. A smaller initial volume would produce a negative volume in the ventricle towards the end of systole, and that is not physiologically possible. It is not uncommon for patients with incompetent pulmonary valves to have a grossly dilated right ventricle.

The pressure-volume loops (PVLs) were obtained by plotting the right ventricular pressure (RVP) against the instantaneous ventricle volume. Figure 4.13 is a set of PVLs for the SJMB valve over a range of PVR between 1.79 and 3.56 mmHg/Lpm. PVC ranged from 2.12 to 4.62 ml/mmHg and CO was maintained between 5.0 and 5.2 Lpm.

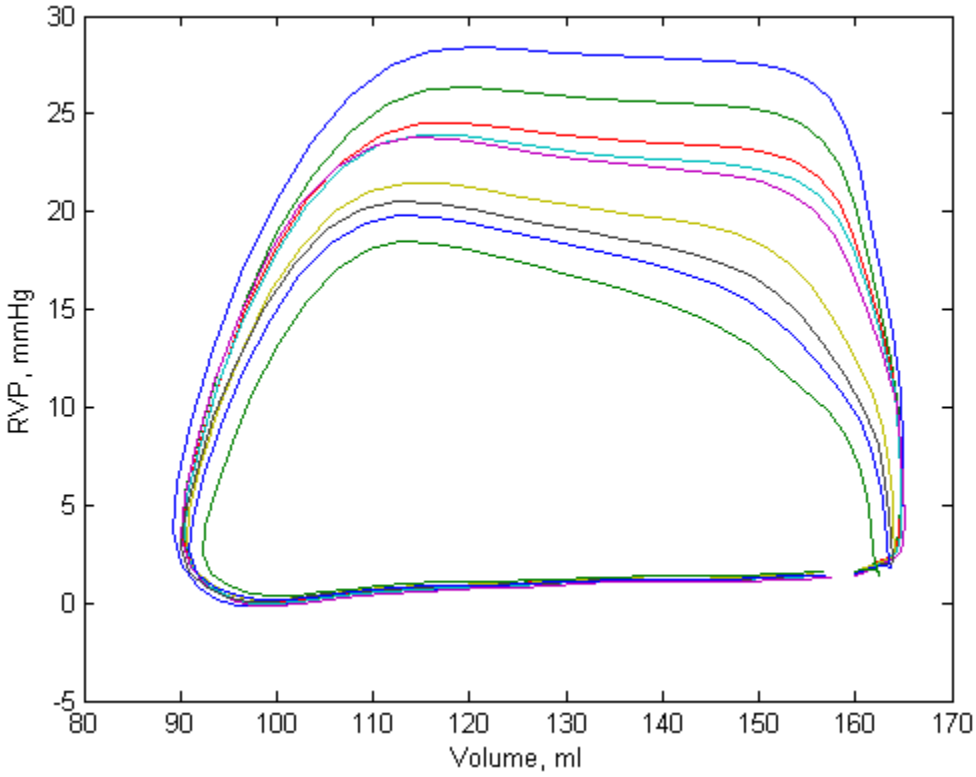

Figure 4.13: Pressure-volume loops for Saint Jude medical bileaflet valve.

In general, the shape of the PVLs in Figure 4.13 are consistent with those of a natural right ventricle (Baker 2009). The smallest PVL in Figure 4.13 corresponds with the lowest PVR. As the PVR increases, so does the size of the PVL. Since ventricular work is defined as the area of the PVL, it is clear that the ventricle responds to an increase in PVR by working harder in order to maintain a stable CO. As illustrated in Figure 4.13, the MPCS in this study has the capability to produce PVLs for a valve prototype over a range of PVR, and from those PVLs, the ventricular work required to produce a consistent CO can be extracted. The small gap in the PLVs is due to a small error in the flow measurements that accumulates through the integration process. The ventricle

volume at the end of a heart cycle should be the same as the initial volume; therefore the small gap illustrates the uncertainty in the volume calculations.

Results for Valve Types Placed in RVOT

Figure 4.14 illustrates the valve placement for the set of tests with the device placed in the RVOT. An adapter was used to hold the diode or stenosis between the contraction of the ventricle and the flow probe.

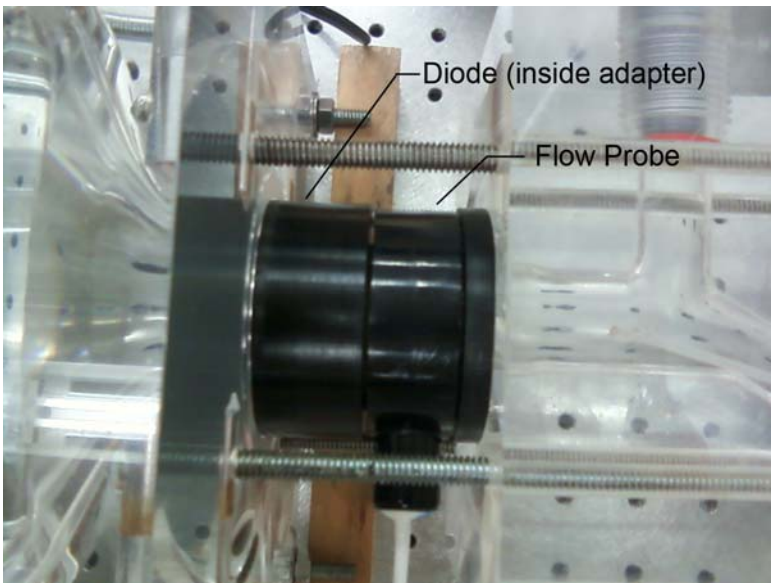

Figure 4.14: Placement of device in the RVOT.

The 60° and 75° diodes and the 0.5 β stenosis were tested in the MPCS under various physiological conditions and compared to each other. Throughout all of the testing, CO was maintained between 5.00 and 5.20 Lpm, and HR was maintained at 75 bpm. Each device was tested multiple times as the MPCS was adjusted to varying levels of PVR. PVC ranged between 1.78 and 3.20 ml/mmHg. The two diodes and the stenosis were compared based on the resulting TVG, RF, and ventricular work.

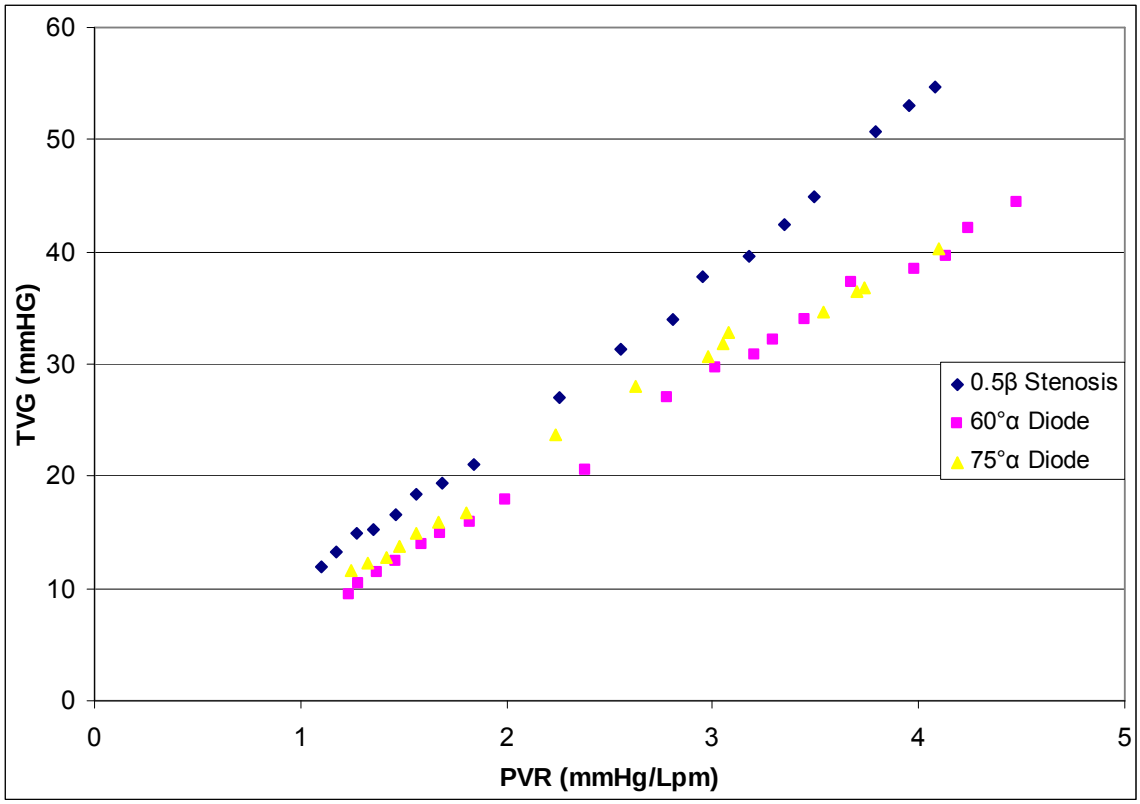

Figure 4.15: Transvalvular gradient vs. resistance for stenosis, 60° and 75° diodes.

Figure 4.15 is the plot of TVG vs. PVR for both diodes and the stenosis and clearly shows a distinct difference in TVG between the stenosis and the diodes, but the TVG of the two diodes are very similar to each other. This was the expected results as both diode designs had the same nozzle-shaped inlet, and a nozzle should produce a lower TVG than a stenosis. To further quantify the differences between the three devices, a 2nd order polynomial regression curve was fit to the data sets using a least-squares regression analysis so that the stenosis and diodes could be directly compared to each other at specific values of PVR. The resulting equations and their corresponding standard error of the fit (s_{xy}) are shown in Table 4.1.

Table 4.1: Regression curve fits for TVG (y) vs. PVR (x) data sets

Valve	2nd Order Polynomial	s_{xy} (mmHg)
0.5β Stenosis	$y = 0.9929x^2 + 9.1438x + 1.1817$	0.498
60°α Diode	$y = -0.1491x^2 + 11.514x - 4.3223$	0.690
75°α Diode	$y = -1.3084x^2 + 17.128x - 8.5568$	0.673

Table 4.2 gives a direct comparison of the TVG at specific PVRs within the tested range. Values for PVR are listed across the top of the chart, the valve types are listed along the left side, and the cells in the middle of the table are the corresponding values for TVG with their 95% confidence interval.

Table 4.2: Direct comparison of TVG (mmHg) vs. PVR (mmHg/Lpm)[1]

	PVR 1.5	PVR 2.0	PVR 2.5	PVR 3.0	PVR 4.0
0.5β Stenosis	17.1±1.03	23.4±1.03	30.2±1.03	37.5±1.03	53.6±1.04
60°α Diode	12.6±1.14	18.1±1.15	23.5±1.15	28.9±1.14	39.3±1.14
75°α Diode	12.2±1.13	20.5±1.14	26.1±1.13	31.1±1.13	39.0±1.13

[1] mean ± uncertainty (95%)

From the data in Table 4.2, it is clear that the diode created a substantially lower TVG than the stenosis. At a low PVR of 1.5 mmHg/Lpm, the TVG of the 60° diode was 26.4% lower than the TVG of the stenosis and 11.1% lower than that of the 75° diode. At a PVR of 3.0 mmHg/Lpm, the TVG of the 60° diode was 23.1% lower than the TVG for the stenosis and 7.00% lower than that of the 75° diode. At a higher PVR of 4.0 mmHg/Lpm, the TVG of the 75° diode was 27.3% lower than the TVG of the stenosis

and 0.830% lower than that of the 60° diode. Clearly both diode designs show significant reduction in TVG over the stenosis, while both diodes perform quite similarly to each other.

Similar results were found regarding RF for the diodes and stenosis. Figure 4.16 is the plot of RF vs. PVR for the stenosis and 60° and 75° diodes.

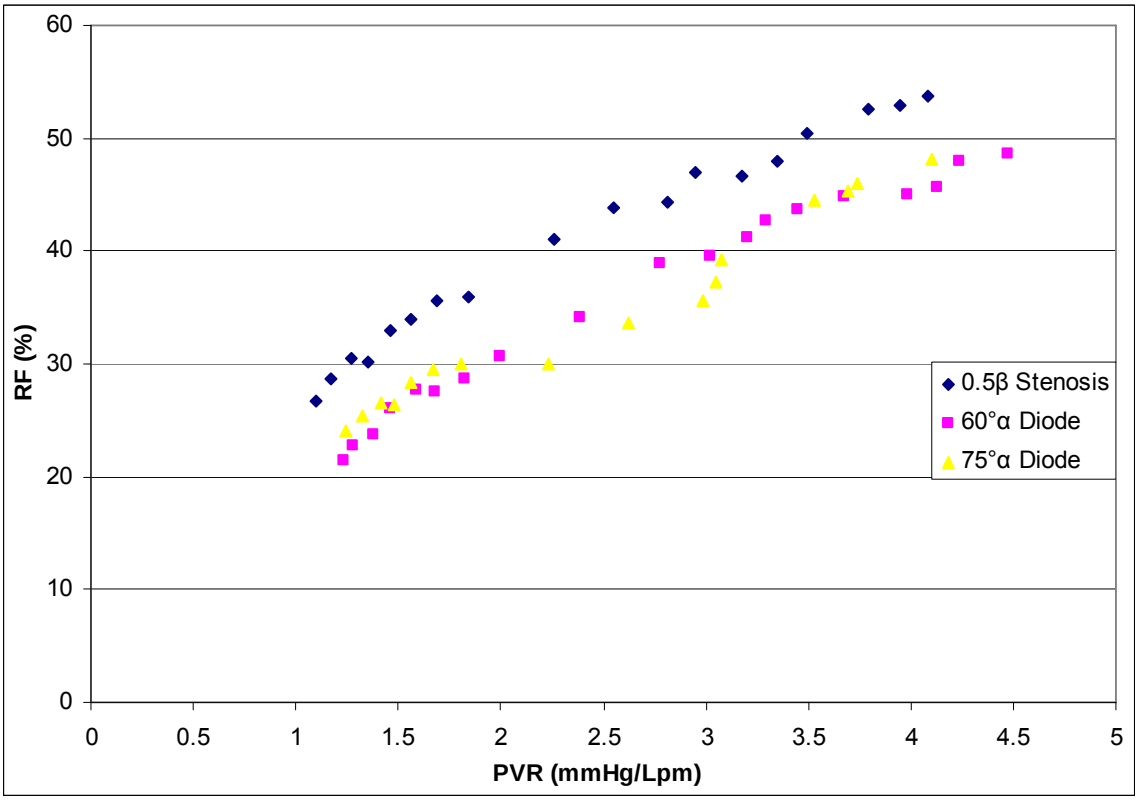

Figure 4.16: Regurgitant fraction vs. resistance for stenosis, 60° and 75° diodes.

This figure illustrates a marked difference in RF between the stenosis and diodes. However, the 60° and 75° diodes had fairly similar RF values over most of the range of PVR. As before, to further quantify the differences between the three devices, a 2nd order polynomial regression curve was fit to the data sets so that the stenosis and diodes could

be directly compared to each other at specific values of PVR. The resulting equations and their corresponding standard error of the fit (s_{xy}) are shown in Table 4.3.

Table 4.3: Regression curve fits for RF (y) vs. PVR (x) data sets

Valve	2nd Order Polynomial	s_{xy} (%)
0.5β Stenosis	$y = -1.2625x^2 + 15.096x + 12.834$	0.830
60°α Diode	$y = -1.3862x^2 + 15.91x + 4.7071$	0.744
75°α Diode	$y = 1.3373x^2 + 1.194x + 22.039$	1.212

Table 4.4 gives a direct comparison of the RF at specific PVRs within the tested range. Values for PVR are listed across the top of the chart, the valve types are listed along the left side, and the cells in the middle of the table are the corresponding values for RF with their 95% confidence interval.

Table 4.4: Direct comparison of RF (%) vs. PVR (mmHg/Lpm)[1]

	PVR 1.5	PVR 2.0	PVR 2.5	PVR 3.0	PVR 4.0
0.5β Stenosis	32.6±2.58	38.0±2.46	42.7±2.27	46.8±2.09	53.0±2.07
60°α Diode	25.5±2.84	31.0±2.79	35.8±2.53	40.0±2.45	46.2±2.61
75°α Diode	26.8±2.44	29.8±2.82	33.4±2.80	37.7±2.64	48.2±2.76

[1] mean ± uncertainty (95%)

From the data in Table 4.4, it is clear that the diodes created a substantially lower RF than the stenosis. At a low PVR of 1.5 mmHg/Lpm, the RF of the 60° diode was 22.0% lower than the RF of the stenosis and 5.16% lower than that of the 75° diode. At a PVR of 3.0 mmHg/Lpm, the RF of the 75° diode was 19.5% lower than the RF of the

stenosis and 5.77% lower than that of the 60° diode. At a higher PVR of 4.0 mmHg/Lpm, the RF of the 60° diode was 12.9% lower than the RF of the stenosis and 4.24% lower than that of the 75° diode. Clearly both diode designs show significant reduction in RF over the stenosis, but performed quite similarly to each other (less than a 5.5% difference in RF).

Ventricular work as a function of PVR for the stenosis and 60° and 75° diodes over a normal range of PVR is shown in Figure 4.17.

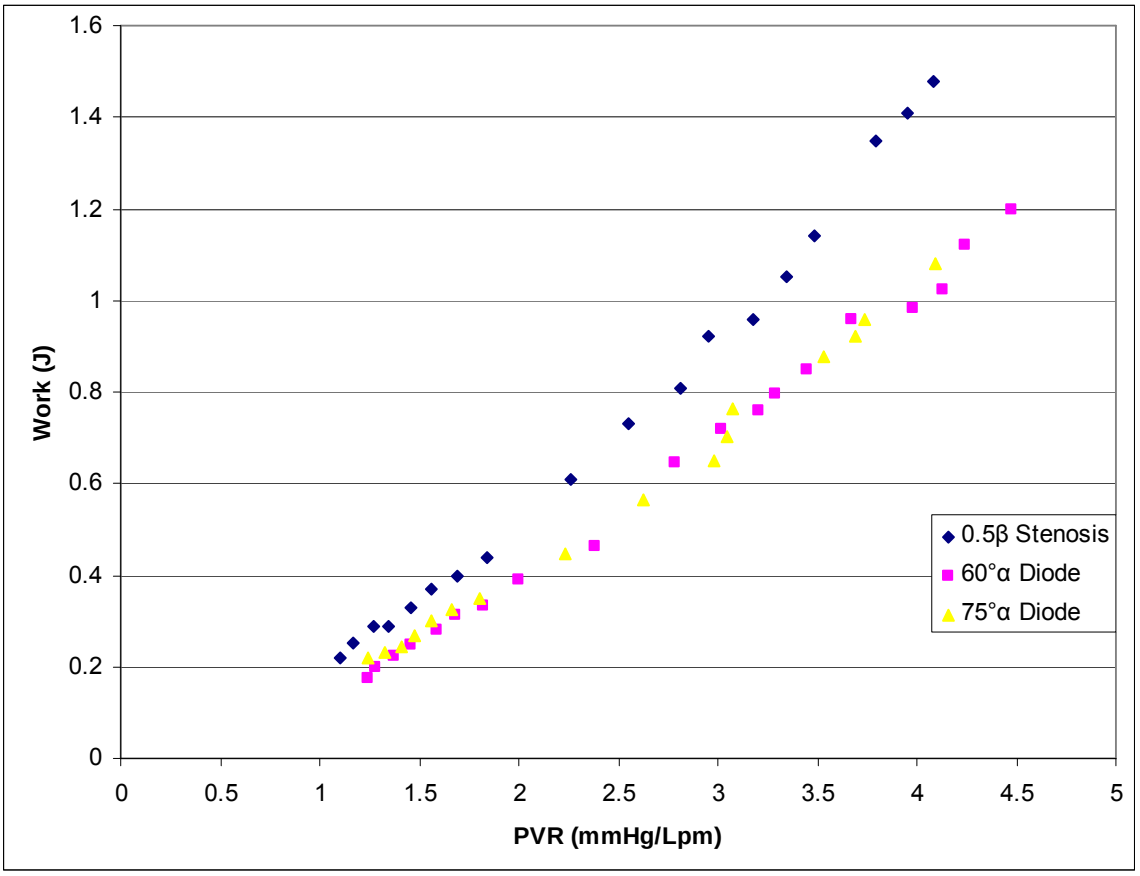

Figure 4.17: Ventricular work vs. resistance for the stenosis, 60° and 75° diodes.

The values in Figure 4.17 illustrate a marked difference in ventricular work between the stenosis and diode. To further quantify the differences between the two devices, a 2nd

order polynomial regression curve was fit to the data sets so that the stenosis and diode could be directly compared to each other at specific values of PVR. The resulting equations, with corresponding standard error of the fit (s_{xy}) are shown in Table 4.5.

Table 4.5: Regression curve fits for Ventricular work (y) vs. PVR (x) data sets

Valve	2nd Order Polynomial	s_{yx} (J)
0.5β Stenosis	$y = 0.0582x^2 + 0.1173x + 0.0343$	0.0200
60°α Diode	$y = 0.0115x^2 + 0.2447x - 0.1392$	0.0234
75°α Diode	$y = 0.0319x^2 + 0.1339x + 0.0008$	0.0168

Table 4.6 gives a direct comparison of the ventricular work for all of the valve prototypes at specific PVRs within the tested range. Values for PVR are listed across the top of the chart, the valve types are listed along the left side, and the cells in the middle of the table are the corresponding values for work with their 95% confidence interval.

Table 4.6: Direct comparison of Ventricular Work (J) vs. PVR (mmHg/Lpm)[1]

	PVR 1.5	PVR 2.0	PVR 2.5	PVR 3.0	PVR 4.0
0.5β Stenosis	0.341±0.0242	0.502±0.0254	0.691±0.0282	0.910±0.0304	1.44±0.0348
60°α Diode	0.254±0.0253	0.396±0.0259	0.544±0.0274	0.698±0.0289	1.02±0.0315
75°α Diode	0.273±0.0254	0.396±0.0271	0.535±0.0280	0.690±0.0294	1.05±0.0309

[1] mean ± uncertainty (95%)

From the data in Table 4.6, it is clear that both diode designs required substantially less ventricular work than the stenosis to achieve the same CO. At a low PVR of 1.5 mmHg/Lpm, the 60° diode performed better than the stenosis and 75° diode.

It required 25.6% less work than the stenosis and 7.20% less work than the 75° diode. At a slightly higher PVR of 2.0 mmHg/Lpm, there was no significant difference in diode performance, but each showed a 21.0% decrease in work from the stenosis for the same CO. At a PVR of 3.0 mmHg/Lpm, the 75° diode performed better. It required 24.2% less work than the stenosis and 1.26% less work than the 60° diode for the same CO. At a higher PVR of 4.0 mmHg/Lpm, the 60° diode performed better. It required 28.7% less work than the stenosis and 2.21% less work than the 75° diode for the same CO. Clearly both diode designs show significant reduction in ventricular work over the stenosis throughout the entire range of PVR. Interestingly, both diodes performed very similarly to each other, with neither design standing out as a more efficient design throughout the range of PVR.

Results for Valve Types Placed in PA

Another set of tests were run to evaluate the performance of the diodes in a position slightly downstream of the RVOT. In this set of tests, data was collected for all three of the diode designs, the stenosis, and also an absent valve case (a blank annulus). Each valve type was placed between the flow probe and the pulmonary artery to simulate placing it 3 cm within the actual artery rather than in the RVTO and tested over a normal range of PVR. PVC ranged between 2.38 and 4.39 ml/mmHg, CO was maintained between 5.00 and 5.20 Lpm, and HR was maintained at 75 bpm.

A qualitative analysis of the work load on the heart for each of the various diodes and stenosis when placed within the pulmonary artery downstream of the RVOT was

accomplished by comparing the PVLs. Several sets of PVLs were obtained for each diode and the stenosis while the MPCS was set for various physiological conditions. Figures 4.18-20 compare the PVLs of the three diodes to each other and to the stenosis. All of the PVLs in each figure were obtained under similar system conditions including CO, HR, and PVR. Since PVR could not be maintained exactly the same for each valve in each experiment, the figures are presented with the average PVR and its standard deviation for that set. CO was maintained between 5.0 and 5.2 Lpm, and HR was maintained at 75 bpm.

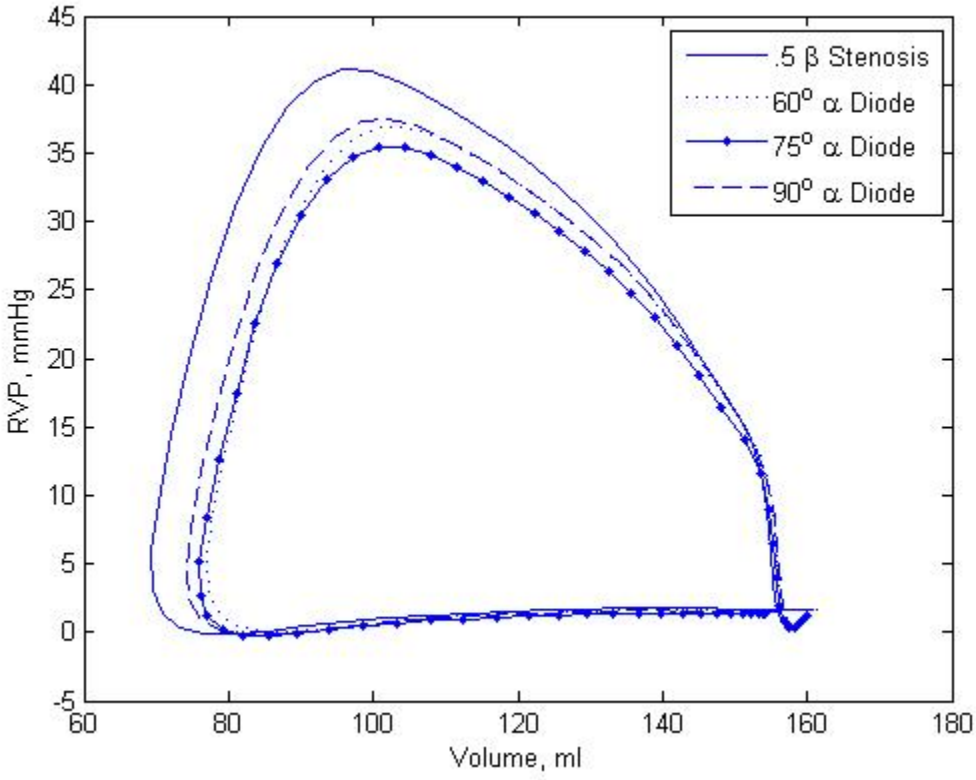

Figure 4.18: PVLs with a PVR of 1.31±0.03 mmHg/Lpm.

Figure 4.18 is comprised of PVLs taken with the system operated at a low, normal PVR. The average PVR for this set of tests is 1.31 mmHg/Lpm with a standard deviation of 0.03 mmHg/Lpm. The range of PVR in this set is 1.27-1.34 mmHg/Lpm. The shape of the PVLs in Figure 4.18 differ from those in Figure 4.13 in that there is no isovolumetric pressure rise at the start of systole. Because the diodes and stenosis allow regurgitant flow, the PAP is able to fall during diastole and ends up being the same pressure as RVP. Therefore forward flow is induced as the very start of systole; whereas with a normal valve the RVP must overcome a higher PAP before forward flow occurs. The shapes of the PVLs in Figure 4.18 are all similar in shape to each other, but it is clear that the 75° diode has the smallest loop, and the stenosis has the largest. This indicates that for this set of tests all of the diodes required less ventricular work than the stenosis, and the 75° diode was the most efficient.

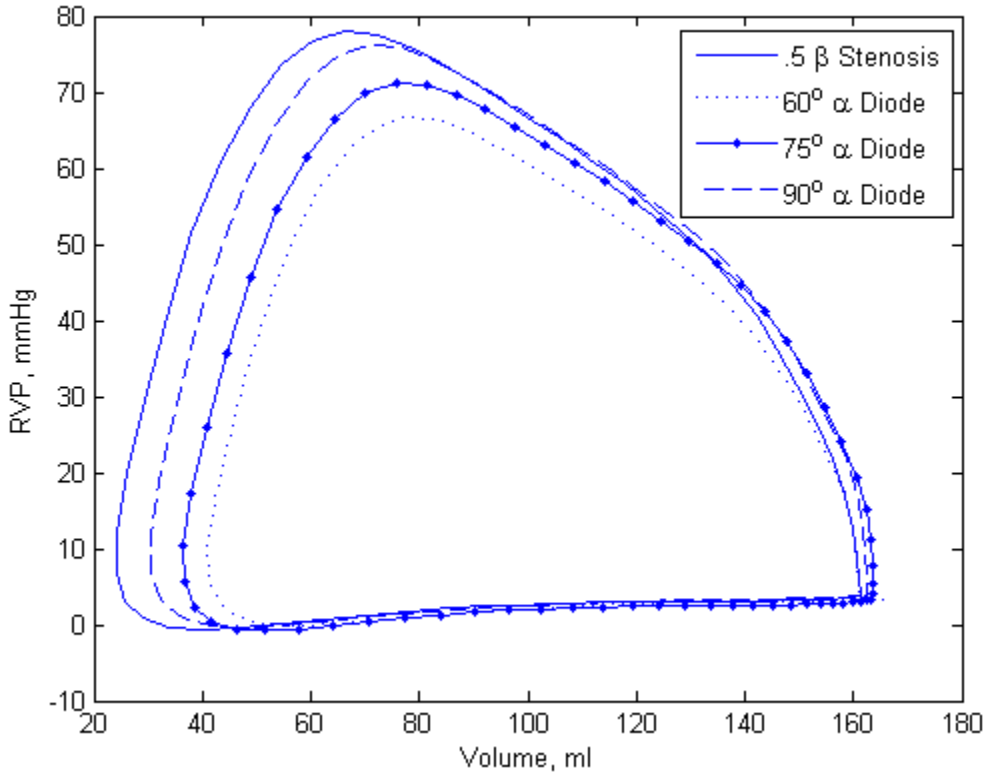

Figure 4.19: PVLs with a PVR of 2.66±0.06 mmHg/Lpm.

Figure 4.19 is comprised of PVLs taken with the system operated at a higher, normal PVR. The average PVR for this set of tests is 2.66 mmHg/Lpm with a standard deviation of 0.06 mmHg/Lpm. The range of PVR in this set is 2.56-2.69 mmHg/Lpm. The PVLs in Figure 4.19 are very similar in shape to those in Figure 4.18. However, the pressures and stroke volumes in Figure 4.19 are much higher and larger. This is to be expected because the ventricle must work much harder to maintain the same CO through a more resistive system. As with Figure 4.18, in Figure 4.19, the stenosis produced the largest PVL, indicating that it is the least efficient. However, unlike Figure 4.18, the

diode that produced the smallest PVL was the 65° diode, indicating that it is the most efficient for this test set.

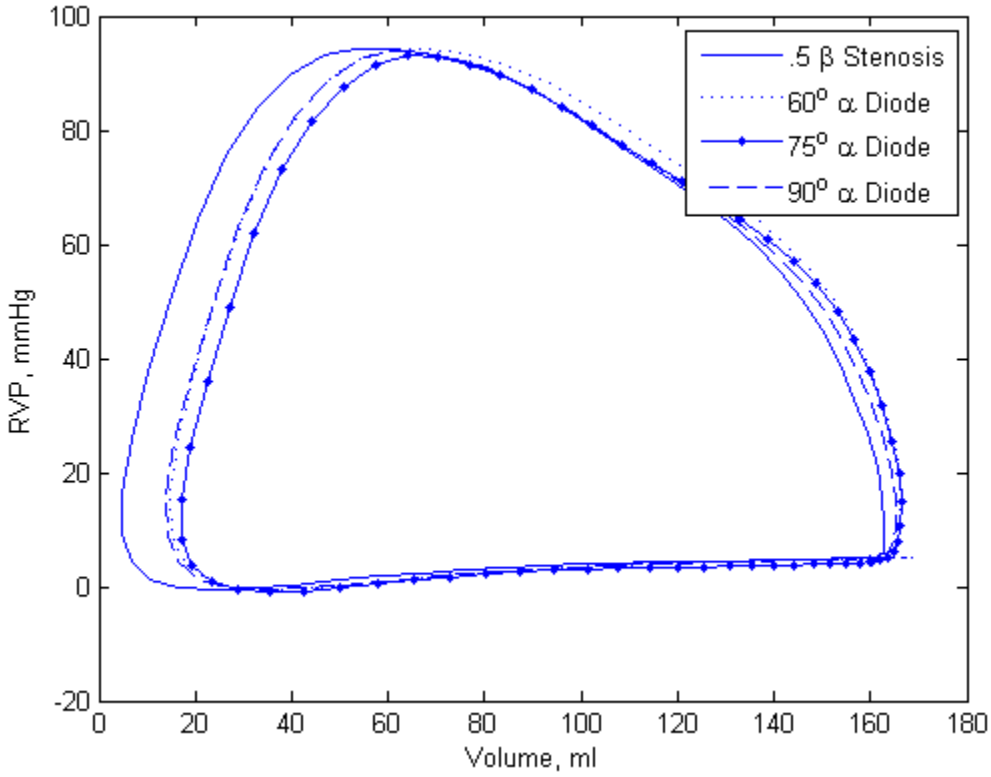

Figure 4.20: PVLs with a PVR of 3.92±0.13 mmHg/Lpm.

Figure 4.20 is comprised of PVLs taken with the system operated at a higher than normal PVR. The average PVR for this set of tests is 3.92 mmHg/Lpm with a standard deviation of 0.13 mmHg/Lpm. The range of PVR in this set is 3.84-4.11 mmHg/Lpm. As with the previous two figures, the 75° diode produced the smallest PVL and the stenosis produced the largest. And due to the increase in PVR, the pressures in the ventricle and the stroke volumes increased from the previous test sets. Figure 4.20 clearly illustrates why the initial ventricle volume was chosen to be 160 ml. The stroke volumes required

for these tests are so large, if the initial volume smaller, the PVL would indicate a negative volume in the ventricle towards the end of systole.

Because of the variability of the PVR and CO for the PVLs in Figures 4.18-20, it is difficult to draw any exact conclusions comparing the efficiency of the diodes based on these figures alone. However, the general trend throughout the figures indicates that all of the diodes produce smaller PVLs than the stenosis, and therefore reduce the workload on the ventricle. A more quantitative analysis between the diodes and stenosis was conducted based on the areas of these PVLs. The area of a PVL defines the work done by the ventricle for that heart cycle. This work was found by integrating the product of the ventricle pressure and downstream flow. Figure 4.21 plots the ventricular work vs. PVR for all of valve options, including the diodes, stenosis, blank annulus, and SJMB valve.

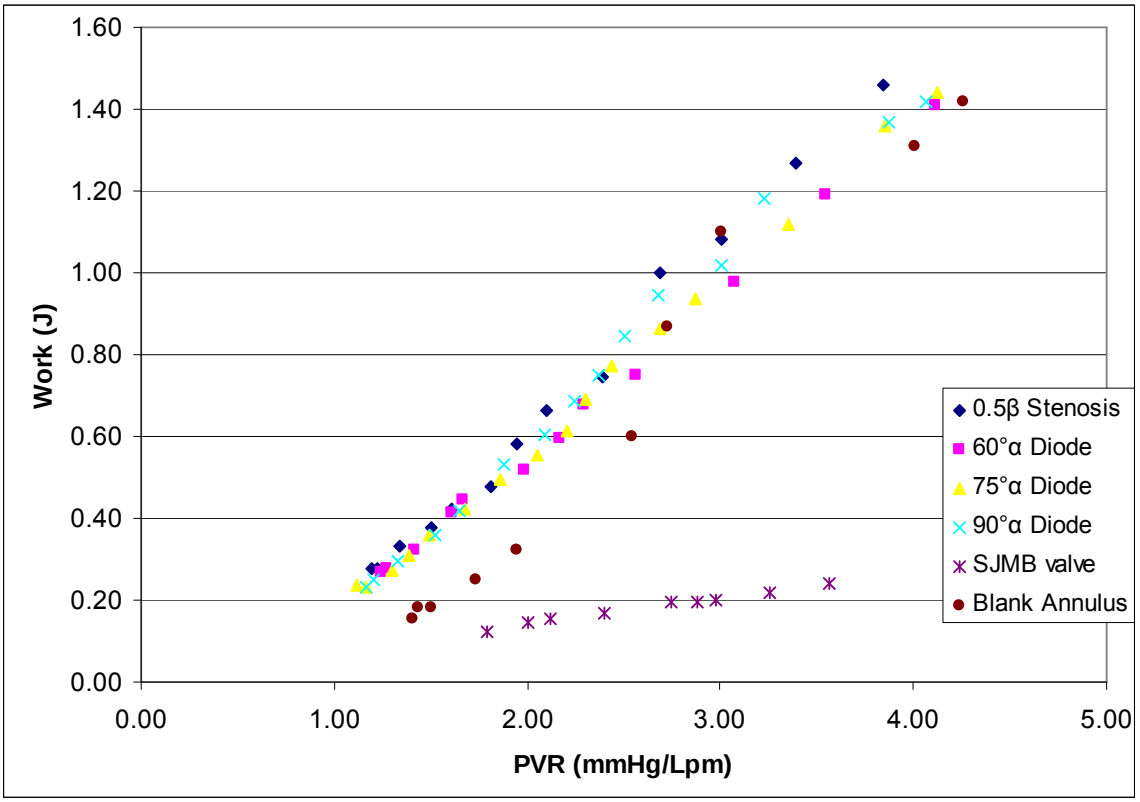

Figure 4.21: Ventricular work vs. PVR for stenosis, diodes, SJMB valve and blank annulus over a range of PVR.

The trends in Figure 4.21 provide a much clearer comparison than individual PVLs. For lower ranges of normal PVR, all three of the diodes function very similarly, and they tend to cause the ventricle to work slightly more efficiently than the stenosis. Interestingly, the blank annulus is more efficient than all of the diodes except when at a PVR of about 3 mmHg/Lpm.

To facilitate a quantitative analysis, a 2nd order polynomial curve was fit to each data set in Figure 4.21 using a least-squares regression analysis. The equations are shown Table 4.7 along with the corresponding standard error of the fit (s_{xy}).

Table 4.7: Regression curve fits for Work (y) vs. PVR (x) data sets

Valve	2nd Order Polynomial	s_{xy} (J)
0.5β Stenosis	$y = 0.0127x^2 + 0.399x - 0.2388$	0.0337
60°α Diode	$y = 0.0156x^2 + 0.318x - 0.1508$	0.0160
75°α Diode	$y = 0.0073x^2 + 0.379x - 0.2247$	0.0199
90°α Diode	$y = -0.0214x^2 + 0.5379x - 0.3886$	0.0309
SJMB Valve	$y = -0.0078x^2 + 0.102x - 0.0304$	0.00406
Blank Annulus	$y = -0.0464x^2 + 0.7244x - 0.8148$	0.0924

Table 4.8 gives a direct comparison of the ventricle workloads for all of the valve prototypes at specific PVRs within the tested range. Values for PVR are listed across the top of the chart, the valve types are listed along the left side, and the cells in the middle of the table are the corresponding values for work with their 95% confidence interval.

Table 4.8: Direct comparison of Ventricular Work (J) vs. PVR (mmHg/Lpm)[1]

	PVR 1.5	PVR 2.0	PVR 2.5	PVR 3.0	PVR 4.0
0.5β Stenosis	0.388±0.0357	0.610±0.037	0.838±0.038	1.073±0.040	1.56±0.042
60°α Diode	0.361±0.0623	0.548±0.063	0.742±0.063	0.945±0.064	1.37±0.066
75°α Diode	0.360±0.0228	0.563±0.024	0.768±0.026	0.978±0.028	1.41±0.031
90°α Diode	0.370±0.0331	0.602±0.034	0.822±0.036	0.103±0.037	1.42±0.039
SJMB Valve	0.105±0.0082	0.142±0.0084	0.176±0.0087	0.205±0.0094	0.253±0.0111
Blank Annulus	0.167±0.0928	0.448±0.0932	0.706±0.0934	0.941±0.0939	1.34±0.0943

[1] mean ± uncertainty (95%)

Based on the values in Table 4.8, all three of the diode designs outperform the stenosis across the entire range of PVR. The 75° diode performs better than the other diodes for a PVR of 1.5 mmHg/Lpm, but with a PVR of 2.0 mmHg/Lpm and higher, the 60° diode performs best of the three diodes. The 90° diode consistently performs the worst of the three diodes, although it always outperforms the stenosis. For a low PVR of 1.5 mmHg/Lpm, the 75° diode requires 7.22% less work than the stenosis and 0.30% less work than the 60° diode. For a PVR of 2.5 mmHg/Lpm, the 60° diode requires 3.48% less work than the 75° diode and 11.5% less work than the stenosis. For a high PVR of 4.0 mmHg/Lpm, the 60° diode requires 2.65% less work than the 75° diode and 12.2% less work than the stenosis.

All three of the diodes perform very closely to each other, and better than the stenosis; although the 75° and 60° diodes consistently performed better than the 90° diodes. In every case the SJMB valve performed the best, requiring up to 81.6% less work than the best diode. Interestingly, the blank annulus was significantly more efficient than all of the diodes over low ranges of PVR, requiring 50.2% less work than the best diode at a PVR of 1.5 mmHg/Lpm.

It was hypothesized that the PVLs and the comparison of ventricular work between the three diodes would provide a clear comparison to determine which one worked best, but the results indicate that the two best diode designs, the 60° and 75° diodes, perform quite similarly to each other. While the 60° diode performed better than the 75° diode for all but the lowest values of PVR, the largest difference between the work loads imposed by the two diodes was only 3.52%.

The diodes did distinguish themselves from the stenosis and the blank annulus in this set of tests based on regurgitant fraction (RF). Figure 4.22 plots the RF of each valve prototype over the same range of PVR.

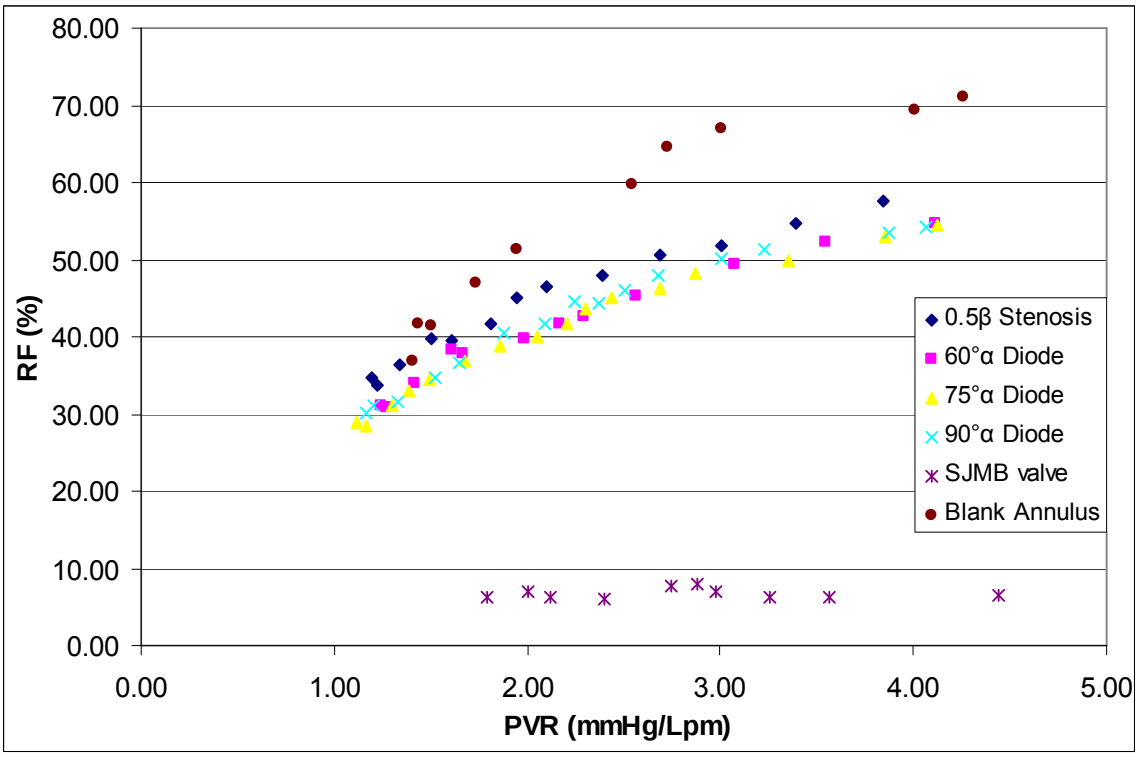

Figure 4.22: Regurgitant Fraction vs. PVR for stenosis, diodes, SJMB valve and blank annulus over a range of PVR.

As seen in Figure 4.22, the diodes clearly produce lower a RF than both the stenosis and the blank annulus. Because the three diodes had slightly varying cusp geometries to impede retrograde flow, it was expected that the three diodes would clearly distinguish themselves from each other based on RF. The diode trends in Figure 4.22 seem to almost overlay each other, so it is difficult to make any conclusions about RF performance simply by observing the figure. Therefore, as with the ventricular work data sets, a 2nd order polynomial curve was fit to each of the data set using the least-squares regression

method. The resulting equations and their corresponding standard error of the fit (s_{xy}) are shown in Table 4.9.

Table 4.9: Regression curve fits for RF (y) vs. PVR (x) data sets

Valve	2nd Order Polynomial	s_{yx} (%)
0.5β Stenosis	$y = -2.0851x^2 + 18.904x + 14.968$	0.898
60°α Diode	$y = -1.6922x^2 + 17.038x + 13.08$	0.922
75°α Diode	$y = -2.0975x^2 + 19.324x + 9.8208$	0.651
90°α Diode	$y = -2.5107x^2 + 21.458x + 8.2524$	0.530
SJMB Valve	$y = -0.4197x^2 + 2.6074x + 2.9276$	0.647
Blank Annulus	$y = -5.0193x^2 + 39.393x - 6.502$	1.428

Table 4.10 gives a direct comparison of the RF for all of the valve prototypes at specific PVRs within the tested range. Values for PVR are listed across the top of the chart, the valve types are listed along the left side, and the cells in the middle of the table are the corresponding values for RF with their 95% confidence interval.

Table 4.10: Direct comparison of RF (%) vs. PVR (mmHg/Lpm)[1]

	PVR 1.5	PVR 2.0	PVR 2.5	PVR 3.0	PVR 4.0
0.5β Stenosis	38.6±2.20	44.4±2.09	49.2±2.04	52.9±1.92	57.2±1.86
60°α Diode	34.8±2.76	40.4±2.57	45.1±2.46	49.0±2.46	54.2±1.95
75°α Diode	34.1±2.57	40.1±2.46	45.0±2.28	48.9±2.56	53.6±1.86
90°α Diode	34.8±2.62	41.1±2.45	46.2±2.82	50.0±2.31	53.9±2.15
SJMB Valve	5.89±2.81	6.46±2.78	6.82±2.82	6.97±2.77	6.64±2.81
Blank Annulus	41.3±2.32	52.2±2.13	60.6±1.96	66.5±1.83	70.8±1.81

[1] mean ± uncertainty (95%)

Based on the values found in Table 4.10, all three diode designs produced a lower RF than both the stenosis and the blank annulus. Naturally the SJMB valve had the lowest RF. At the low PVR of 1.5 mmHg/Lpm, the 75° diode performed better than the other diodes. The RF of the 75° diode was 17.5% lower than that the blank annulus, 11.8% lower than that of the stenosis, and 2.02% lower than that of the next-best diode. At a PVR of 3.0 mmHg/Lmp, the 60° and 75° diodes had nearly the same RF (within 0.1% difference), which was 26.5% lower than that of the blank annulus, 7.56% lower than that of the stenosis, and 2.23% lower than that of the 90° diode. At the high PVR of 4.0 mmHg/Lpm, the 75° diode performed better than the other diodes. The RF of the 75° diode was 24.3% lower than that of the blank annulus, 6.41% lower than that of the stenosis, and 0.660% lower than that of the next best diode, which for this PVR was the 90° diode. All three of the diodes performed quite similarly to each other in regards to RF, and no particular design was significantly better than another.

The comparison of TVG for the diodes, stenosis, blank annulus, and SJMB valve across a range of PVR is shown in Figure 4.23.

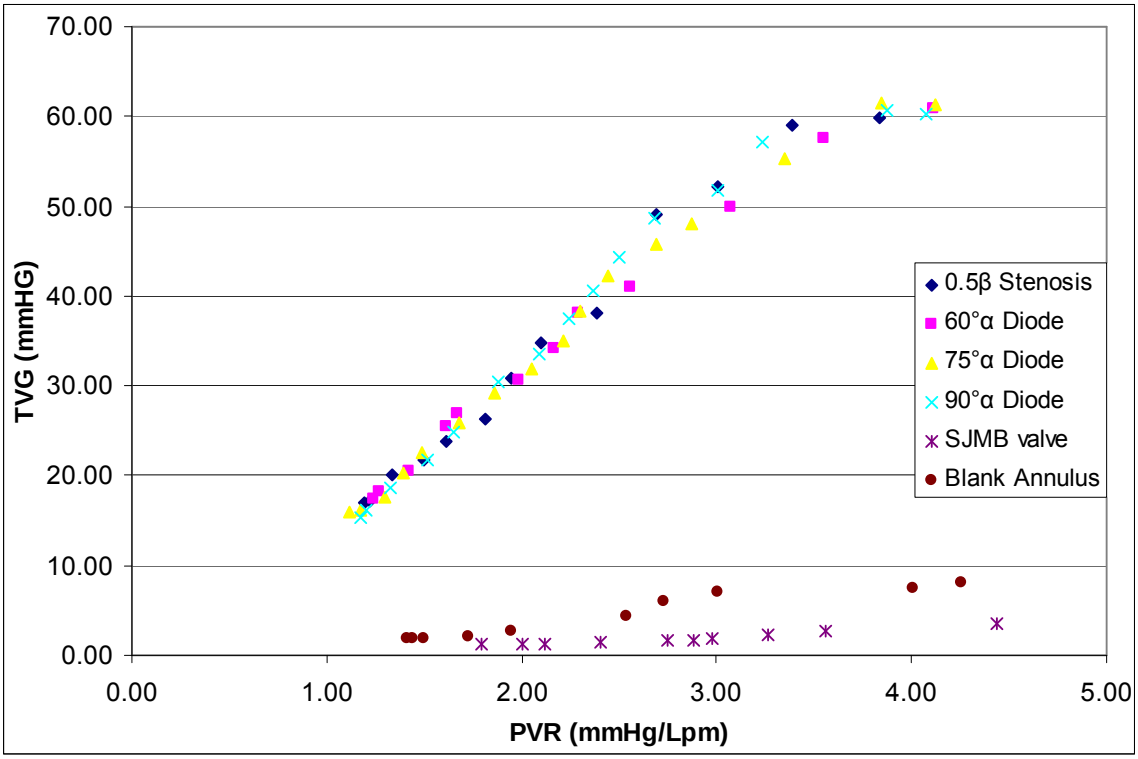

Figure 4.23: Transvalvular Gradient vs. resistance for stenosis, diodes, SJMB valve and blank annulus over a range of PVR.

Since all three of the diode designs had the exact same inlet geometry, it was expected that they all would produce the same TVG. Figure 4.23 clearly indicates that all of the diodes do indeed produce nearly the same TVG across a range of PVR. Also, as expected, the blank annulus produced the lowest TVG because there is nothing in the way to impede antegrade flow. To better quantify the similarities and differences between the valve types, a 2nd order polynomial curve was fit to the data sets. The resulting equations and the corresponding standard error of fit (s_{yx}) are show in Table 4.11.

Table 4.11: Regression curve fits for TVG (y) vs. PVR (x) data sets

Valve	2nd Order Polynomial	s_{yx} (mmHg)
0.5β Stenosis	$y = -2.0701x^2 + 28.151x - 15.064$	2.131
60°α Diode	$y = -1.9894x^2 + 26.232x - 12.229$	1.070
75°α Diode	$y = -2.1813x^2 + 27.678x - 13.872$	1.200
90°α Diode	$y = -3.6042x^2 + 35.43x - 22.507$	1.589
SJMB Valve	$y = 0.1885x^2 - 0.2091x + 0.9019$	0.153
Blank Annulus	$y = -0.509x^2 + 5.2086x - 4.8901$	0.557

Table 4.12 gives a direct comparison of the TVG for all of the valve prototypes at specific PVRs within the tested range. Values for PVR are listed across the top of the chart, the valve types are listed along the left side, and the cells in the middle of the table are the corresponding values for TVG with their 95% confidence interval.

Table 4.12: Direct comparison of TVG (mmHg) vs. PVR (mmHg/Lpm)[1]

	PVR 1.5	PVR 2.0	PVR 2.5	PVR 3.0	PVR 4.0
0.5β Stenosis	22.5±2.32	33.0±2.32	42.4±2.32	50.8±2.32	64.4±2.32
60°α Diode	22.6±1.40	32.3±1.40	40.9±1.40	48.6±1.41	60. 9±1.41
75°α Diode	22.7±1.50	32.8±1.50	41.7±1.51	49.5±1.51	61.9±1.51
90°α Diode	22.5±1.83	33.9±1.83	43.5±1.83	51.3±1.83	61.5±1.83
SJMB Valve	1.01±0.918	1.24±0.918	1.56±0.918	1.97±0.919	3.08±0.919
Blank Annulus	1.78±1.06	3.49±1.06	4.95±1.06	6.16±1.06	7.80±1.06

[1] mean ± uncertainty (95%)

From Table 4.12, it is clear that all of the diodes performed similarly to each other, with less than 6.1% difference in TVG over all of the tests. The results that are not as expected are that the diodes demonstrated no significant improvement in TVG compared to the stenosis (less than 6% difference throughout the entire range of PVR tested). In fact, a few of the results indicate the stenosis as having a lower TVG than some of the diodes. It was expected that the stenosis, which acts simply as an orifice, would produce a significantly higher TVG than the diodes, which have a nozzle-shaped inlet, as was the case when the devices were placed in the RVOT. The fact that the diodes and the stenosis act so similarly during systole for this set of tests indicates that the performance of the diode is also a function of its placement in the MPCS. Obviously placing the diode several centimeters downstream of the RVOT greatly reduces the effectiveness of the diode. It is suspected that for these tests, the short entrance length between the RVOT and the inlet of the diode altered the flow profile entering the diode, which reduced the nozzle effect of the diode during systole. Another possible explanation for the increased TVG with the diode placed in the artery is that although the diode was moved 3 cm downstream, the catheter used to collect PAP was not moved. As the fluid enters the nozzle, it experiences a significant pressure drop as the velocity increases. The pressure rises to the actual PAP as the jet dissipates. If the pressure tap in the catheter is too close to the diode then the PAP would appear to be lower than it actually is. A lower PAP would results in a larger TVG.

The results of both sets of tests indicate that the placement of the diode within the test section greatly affects its performance. Over the range of PVR from 1.5 to 4.0

mmHg/Lpm, the 60° diode required between 25.7% and 31.9 % less work with it placed in the RVOT immediately at the contraction of the ventricle than it did with it placed 3 cm downstream. Evidently, to be most effective, the diode must be placed immediately at the contraction of the ventricle in the MPCS, and be placed in the annulus of the pulmonary artery in a real pulmonary system.

Overall, the results of this study indicate a higher RF for all of the valve types than was expected. Camp (2009) reported a much lower RF for the diodes she tested as well as for a blank annulus. In a benchmark paper, Kilner et al., (2008) reported some values for RF below 35% for a blank annulus. However, the findings in this study do not necessarily contradict those found by Kilner et al. Some major differences between the studies are probable cause for the incongruent results. The values for proximal resistance used by Kilner et al., were much larger than the proximal resistance in the MPCS of this study. The proximal resistance in this study's MPCS (between the pulmonary artery annulus and the windkessel) was measured as 0.120 mmHg/Lpm through the right branch and 0.160 mmHg·s/l through the left branch. As these resistances are in parallel, the total proximal resistance is 0.0690 mmHg/Lpm. Kilner et al., used a resistance of 0.0833 mmHg/Lpm in the main pulmonary artery and a resistance of 0.250 mmHg/Lpm in the pulmonary artery branches. These two resistances are in series; therefore Kilner's total proximal resistance was 0.333 mmHg/Lpm, almost five times larger than that of this study. As the Kilner et al., model predicts that reducing the resistance upstream of the compliance elements results in an increased RF, it follows that the MPCS of this study would produce a larger RF. Also, Kilner et al., kept the stroke volume of their ventricle

constant, so that as distal resistance was raised, or as proximal resistance was lowered, the cardiac output was allowed to fall. In this study, the cardiac output was maintained throughout the entire range of PVR by means of raising stroke volume. With a greatly increased stroke volume, it follows that the RF would also increase. Several modifications made to Camp's MPCS (such as enlarging the hose connections on the pulmonary artery test section and shortening the length of tubing between the artery and windkessels) reduced the proximal resistance. Therefore it follows that the RF results in this study would be greater than those found by Camp.

CHAPTER FIVE

CONCLUSIONS

The primary objectives of this study were: (1) to conduct a flow visualization with four diode geometries to evaluate their flow in a pulsatile system, and (2) to evaluate three diode geometries *in vitro* in a mock pulmonary circulatory system (MPCS) based on their ventricular work, regurgitant fraction, and transvalvular gradient.

A two-dimensional test section was developed and built for the purpose of objective (1). Through flow visualization, all four of the diode designs tested performed very similarly to each other in both systole and diastole. During systole, each diode created a strong jet that spanned the entire distance between the two cusps. No *vena contracta* was evident during systole for any of the designs. During diastole each diode created a *vena contracta* which reduced the effective area of the diode. The diode with the 75° apex angle reduced the effective flow area the most, from 654 mm^2 to 335 mm^2, a 48% reduction.

Three diodes, with varying cusp geometries were designed and machined for this study. A novel pneumatic ventricle was designed and built for this study, and an existing MPCS was modified to accommodate the new ventricle. Other modifications of the MPCS were made to improve performance and measurement capabilities, such as the placement of a flow probes both upstream and downstream of the ventricle. From the flow and pressure data, PVLs were obtained, and ventricular work, regurgitant fraction (RF), and transvalvular gradient (TVG) were calculated. These results provided a means

by which to compare the three diodes to each other as well as to a comparable stenosis and a blank annulus.

The results of the set of tests in which the devices were placed in the RVOT indicate that the 60° and 75° diodes perform very similarly to each other based on ventricular work, RF, and TVG. Neither of the two designs distinguished itself as significantly better than the other. However, the results indicate that both diodes are a significant improvement over the 0.5 β stenosis, reducing RF by up to 22.0%, TVG by up to 27.3%, and ventricular work by up to 28.7%.

The results of the set of tests in which the devices were placed 3 cm downstream of the RVOT, within the pulmonary artery, indicate that all three of the diodes performed very similarly to each other in this position as well. None of the diodes significantly distinguished itself from the others based on any parameter results. However, when placed in this position, the diodes became significantly less effective than they had been in the RVOT. The diode with the lowest RF was only an 11.7% improvement over the stenosis. For some values of PVR, the stenosis actually had a lower TVG than some of the diodes. The diode that required the least ventricular work was only up to a 13.9% improvement over the stenosis. Such remarkably different results between the two sets of test indicate that the placement of the diode in relation to the contraction of the ventricle greatly affects the diode's performance.

While placed in the RVOT, the 60° diode produced a RF between 25.5% and 46.2%. Therefore for a patient with a lower PVR, the diode produces an acceptable level of regurgitation. However, above a PVR of about 2.5 mmHg/Lpm, the RF is higher than

acceptable. For a PVR of 3.0 mmHg/Lpm the 60° diode produced a TVG of 28.9 mmHg, which is acceptable. However, at PVRs above that, the TVG is larger and unacceptable.

The results of this study strongly indicate that the placement of the diode greatly affects its performance, and that the diode must be place at the annulus of the pulmonary artery to be most effective. The results of the set of tests with the diode placed in the RVOT suggest that the diode may be a suitable candidate as a replacement for a stenosed valve providing the patient has a PVR below 2.5 mmHg/Lpm. More research should be conducted to improve diode design and performance.

Recommendations

Many modifications were made to the MPCS used in this study. While all of the modifications were beneficial to the system in some way, some modifications also ended up detracting from the system. Removing the flow probes between the pulmonary artery branches and the downstream compliance elements helped to reduce the resistance and inertance in the system; however, removing them also eliminated the ability to accurately balance the flow between the two artery branches. A recommendation for a system using a rigid artery test section would be to place a flow probe between each artery branch and the downstream compliance elements. However, it is also recommended that future research be conducted with a compliant pulmonary artery test section, as it would be more physiological. If future research does involve using a compliant artery test section, the downstream flow probe must again be placed upstream of the test section. One last

recommendation is to replace the current downstream resistance element with a linear resistance element, which would be more physiological.

The marked differences in the results between the two sets of testing in the MPCS indicate that the placement of the diode within the system has as much effect on its performance as the actual design of the diode. This is an important lesson to be considered during further research in this area. When placed immediately at the contraction of the ventricle, the diode affected the flow as it was designed to, and the result was a significantly lower work load on the ventricle as compared to the stenosis.

Appendix A

Uncertainty Analysis

Every result of the *in vitro* testing in this study was extracted from the flow and pressure measurements taken in the MPCS. Therefore, to quantify the uncertainty of those results, the uncertainty of the flow and pressure data was determined, and an uncertainty analysis was performed to determine how those errors propagate into the final results. Methods described by Figliola and Beasley (2005) were used for the analysis. Elemental errors for each component were identified, the magnitudes of systematic and random errors were estimated, and the uncertainty estimate for the results was calculated. Uncertainty estimates were determined for pulmonary vascular resistance, pulmonary vascular compliance, transvalvular gradient, regurgitant fraction, and ventricular work.

Sources of Error

Sources of error in the flow and pressure data stem from the following: calibration, data acquisition, and data reduction. These errors can be either random or systematic in nature. In a multiple-measurement uncertainty analysis, random errors within a set of data are accounted for by the random scatter of the data and are given by the standard uncertainty,

$$\left(s_{\bar{x}}\right)_k = s_{x_k} \Big/ \sqrt{N_k} \tag{A.1}$$

where s_x is the standard deviation of the data, and N is the number of samples taken. For instance, to determine the random error in a mean flow measurement while analyzing 25

cycles of data, s_x would be the standard deviation of the mean flows for the 25 cycles, and N would be 25. Random uncertainties are combined using the root-sum-squares method (RSS). Systematic uncertainties, $\left(b_{\bar{x}}\right)_k$, are combined together using the RSS method. The total uncertainty at a 95% confidence level is reported as

$$u_x = \pm t_{95}\left(b_{\bar{x}}^2 + s_{\bar{x}}^2\right)^{1/2}(95\%)\,. \qquad \text{(A.2)}$$

t_{95} is the weighting function for 95% confidence found as $f(\nu,95)$ from the Student t distribution where ν is the degrees of freedom, and ν = N-1. In this study, N = 25 because each reported value for pressure and flow was averaged over 25 cycles.

Elemental Errors in Flow and Pressure Measurements

Errors in the upstream flow ($Q_{upstream}$) and downstream flow ($Q_{downstream}$) measurements are introduced from several elements. Uncertainty in the flow meters' zero setting introduces a systematic error whose uncertainty is assigned b_1, For both $Q_{upstream}$ and $Q_{downstream}$, $b_1 = 0.050$ Lpm. All random errors originating from the calibration process are accounted for by the random error of the calibration curve fit, which is assigned the random uncertainty $s_1 = s_{yx}$ based on the standard error of the curve fit (See Equation A.10). The random error due to variations between cycles in the data set is assigned the standard random uncertainty $s_2 = \frac{s}{\sqrt{N}}$, or the standard deviation of the mean flow rates. The random uncertainty s_1 was found to be 0.061 Lpm and 0.043 Lpm for $Q_{upstream}$ and $Q_{downstream}$ respectively. The random uncertainty s_2 varied for both

$Q_{upstream}$ and $Q_{downstream}$ between data sets. Table A.1 summarizes the errors in the flow measurements and their assigned uncertainties.

Table A.1: Errors and uncertainties in all flow measurements

Uncertainty	Error	Assigned uncertainty $Q_{upstream}$, $Q_{downstream}$
b_1	shift in zero point	0.050 Lpm, 0.050 Lpm
s_1	calibration/instrument error	0.061 Lpm, 0.043 Lpm
s_2	random scatter between cycles of data	varies between data sets

Several elemental errors contribute to uncertainties in the pressure measurements. A systematic error per the manufacturer's specification is assigned a standard systematic uncertainty, b_1. All random errors originating from the calibration process, including sensor and instrument resolution, are accounted for by the random error of the calibration curve fit, which is assigned the random uncertainty $s_1 = s_{yx}$ based on the standard error of the curve fit (See Equation A.10). The random error due to variations between cycles in the data set is assigned the standard random uncertainty $s_2 = \frac{s}{\sqrt{N}}$, or the standard deviation of the mean pressures. Uncertainty in the pressure transducers' zero setting introduces a systematic error whose uncertainties (b_{RVP} *and* b_{PAP}) for *RVP* and *PAP* respectively were observed to be about 0.200 mmHg. The random uncertainty s_1 was found to be 0.161 mmHg and 0.324 mmHg for *RVP* and *PAP* respectively. The random uncertainty s_2 varied for both *RVP* and *PAP* between data sets. Table A.2 summarizes the errors in the flow measurements and their assigned uncertainties.

Table A.2: Errors and uncertainties in all pressure measurements

Uncertainty	Error	Assigned uncertainty *RVP* , *PAP*
b_1	shift in zero point	0.200 mmHg, 0.200 mmHg
s_1	calibration/instrument error	0.161 mmHg, 0.324 mmHg
s_2	random scatter between cycles of data	varies between data sets

Pulmonary Vascular Resistance

A spectral analysis of the pressure and flow data was used to calculate PVR. However, it was the zeroth harmonic of the impedance spectrum (*Z*), which is simply the average pressure over the average flow, that yields PVR. Therefore the following is used to analyze error propagation into PVR measurements:

$$u_{PVR} = \sqrt{\left(\frac{\partial Z}{\partial PAP} u_{PAP}\right)^2 + \left(\frac{\partial Z}{\partial Q} u_Q\right)^2} \tag{A.3}$$

where $\frac{\partial Z}{\partial PAP} = \frac{1}{Q}$ and $\frac{\partial Z}{\partial Q} = -\frac{PAP}{Q^2}$. The uncertainties u_{PAP} and u_Q in Equation A.3 are the 95% confidence level uncertainties of *PAP* and $Q_{downstream}$, found by combining the respective systematic and random uncertainties as shown in Equation A.2. In this study, the final uncertainties for PVR were typically about ± 0.18 mmHg/Lpm (95%).

Pulmonary Vascular Compliance

The impedance spectrum was also used to determine PVC. However, for convenience, the uncertainty analysis for PVC was conducted based on the clinical

method for determining PVC. It is assumed that the spectral method would have even less uncertainty than the clinical method. Based on the clinical formula for PVC (see Equation 4.2) the 95% confidence level uncertainty in PVC was determined with

$$u_{PVC} = \sqrt{\left(\frac{\partial PVC}{\partial CO}u_{CO}\right)^2 + \left(\frac{\partial PVC}{\partial PAP_{pulse}}u_{PAP_{pulse}}\right)^2 + \left(\frac{\partial PVC}{\partial HR}u_{HR}\right)^2} \qquad \text{(A.4)}$$

where $\frac{\partial PVC}{\partial CO} = \frac{1000}{PAP_{pulse} \cdot HR}$, $\frac{\partial PVC}{\partial PAP_{pulse}} = \frac{-CO \cdot 1000}{PAP_{pulse}^2 \cdot HR}$, and $\frac{\partial PVC}{\partial HR} = \frac{-CO \cdot 1000}{PAP_{pulse} \cdot CO^2}$.

Heart rate, which was 75.00 bpm in every data set in this study, had negligible uncertainty; therefore u_{HR} is assigned zero. The uncertainty u_{CO} is found by combining the systematic uncertainty of Q with the random uncertainty of $Q_{downstream}$ as in Equation A.2. In this study, the final uncertainties for PVC were typically about ± 0.18 ml/mmHg (95%).

Transvalvular Gradient

TVG is determined by

$$TVG = RVP_{peak} - PAP_{peak}. \qquad \text{(A.5)}$$

The 95% confidence level uncertainty for TVG is found by

$$u_{TVG} = \sqrt{\left(\frac{\partial TVG}{\partial RVP}u_{RVP}\right)^2 + \left(\frac{\partial TVG}{\partial PAP}u_{PAP}\right)^2} \qquad \text{(A.6)}$$

Where $\frac{\partial TVG}{\partial RVP} = 1$ and $\frac{\partial TVG}{\partial PAP} = -1$. The uncertainties u_{RVP} and u_{PAP} are determined by Equation A.2.

TVG results reported in Tables 4.2 and 4.12 were determined using a regression curve fit to the data set. This method introduced a random data-reduction error which is assigned the random uncertainty $s_3 = s_{yx}$ based on the standard error of the curve fit (See Equation A.10). This random uncertainty is combined with u_{TVG} using the RSS method. In this study, the uncertainty in TVG was between ± 1.0 and 1.5 mmHg (95%) when the devices were placed in the RVOT and between ± 1.0 and 2.5 mmHg (95%) when they were placed further downstream within the artery.

Regurgitant Fraction

RF is defined as mean reverse flow over mean forward flow (see Equation 3.3); therefore the uncertainty in RF propagates as the following:

$$u_{RF} = \sqrt{\left(\frac{\partial RF}{\partial Q_F} u_{Q_F}\right)^2 + \left(\frac{\partial RF}{\partial Q_R} u_{Q_R}\right)^2} \tag{A.7}$$

Where $\frac{\partial RF}{\partial Q_F} = \frac{-100 \cdot Q_R}{Q_F^2}$ and $\frac{\partial RF}{\partial Q_R} = \frac{100}{Q_F}$. The uncertainties u_{Q_F} and u_{Q_R} are determined by Equation A.2.

RF results reported in Tables 4.4 and 4.10 were determined using a regression curve fit to the data set. This method introduced a random data-reduction error which is assigned the random uncertainty $s_3 = s_{yx}$ based on the standard error of the curve fit (See Equation A.10). This random uncertainty is combined with u_{RF} using the RSS method. In this study, the final uncertainty for RF is typically around ± 2.50% (95%), but always under ± 3.00% (95%).

Ventricular Work

Ventricular work was found by integrating the product of RVP and instantaneous flow into the ventricle over an entire heart cycle. For this uncertainty analysis, it will suffice to let the ventricular work be found by the following:

$$W = \sum_{i=1}^{n} RVP_i \cdot Q_i \cdot dt \tag{A.8}$$

where n=64 as there was 64 data points taken per heart cycle. dt is 0.0125 s, but has no known uncertainty in this study. As the uncertainties in RVP and Q are known for any particular data point, let n=1 and those uncertainties will propagate into the work as

$$uW_1 = \sqrt{\left(\frac{\partial W_1}{\partial RVP_1} uRVP\right)^2 + \left(\frac{\partial W_1}{\partial Q_1} uQ\right)^2} \ . \tag{A.9}$$

Peak values for RVP and Q are used so that the maximum uncertainty for any time step in the cycle is determined. This uncertainty is then multiplied by the number of time steps in a cycle to determine the maximum combined uncertainty, u_W.

Ventricular Work results reported in Table 4.6 and 4.8 were determined using a regression curve fit to the data set. This method introduced a random data-reduction error which is assigned the random uncertainty $s_3 = s_{yx}$ based on the standard error of the curve fit (See Equation A.10). This random uncertainty is combined with u_W using the RSS method.

Least-Squares Regression Analysis

A least-squares regression analysis was used to compare RF, TVG, and ventricular work data for each valve type (See Tables 4.1-4.12). The polyfit function in Matlab was used to fit a 2nd order polynomial to each data set. The standard error of the fit (s_{yx}) was found by

$$s_{yx} = \sqrt{\frac{\sum_{i=1}^{N}(y_i - y_{ci})^2}{\nu}} \tag{A.10}$$

where ν is the degrees of freedom of the fit.

REFERENCES

Alexander R, *Hurst's The Heart*. 9th ed. 1998. New York: McGraw-Hill.

Baker H, "Ventricular pressure/volume loop analysis: from bench to bedside." Lecture given at Clemson University. 02 February 2011.

Bean H, *Fluid Meters: Their Theory and Application*. 6 ed. 1971. New York: ASME.

Bloomfield P, "Choice of heart valve prosthesis." *Heart*, 2002. **87**:583-9.

Berne R and Levy M, *Cardiovascular Physiology*. 1992. Boston: Mosby Year Book.

Burkhoff D, Mirsky I, and Suga H, "Assessment of systolic and diastolic ventricular properties via pressure-volume analysis: A guide for clinical, translational, and basic researchers." *Am J Physiol. Heart Circ Physiol*, 2005. **289**: H501-12.

Camp TA, "Evaluation of fluid diodes for use as pulmonary heart valve replacements," in PhD thesis. 2009, Clemson University

Camp TA, Stewart KC, Figliola RS, and McQuinn T, "In Vitro Study of Flow Regulation for Pulmonary Insufficiency." *ASME J Biomechanical Engineering*, 2007. **129**(2).

Chang BC, Lim SH, Kim DK, Seo JY, Cho SY, Shim WH, Chung N, Kim SS, and Cho BK, "Long-term results with St. Jude Medical and CarboMedics prosthetic heart valves." *J Heart Valve Dis*, 2001. **10**(2):185-94; discussion195.

Culbreath C, "Fluid diode for pediatric pulmonary artery insufficiency." Honors BS Thesis. Clemson University, 2004.

Deviri E, Sareli P, Wisenbaugh T, and Cronje SL, "Obstruction of mechanical heart valve prostheses: clinical aspects and surgical management." *J Am Coll Cardiol*, 1991. **17**(3):646-50.

Emery RW, Erickson CA, Arom KV, Northrup WF, Kersten TE, Von Rueden TJ, Lillehei TJ, and Nicoloff DM, "Replacement of the aortic valve in patients under 50 years of age: long-term follow-up of the St. Jude Medical prosthesis." *Ann Thorac Surg*, 2003. **75**(6):1815-9.

Figliola RS, “A Study of the Hemolytic Potential of Prosthetic Heart Valve Flows Based on Local In Vitro Stress Measurements.” 1976, Notre Dame.

Figliola RS, and Beasley D, *Theory and Design for Mechanical Measurements*. 4th ed. 2005. New York: Wiley.

Fukada J, Morishita K, Komatsu D, and Abe T, “Influence of pulmonic position on durability of bioprosthetic heart valves.” *Ann Thorac Surg*, 1997. **64**(6):1678-80; discussion 1680-1.

Gohean J, Figliola R, Camp T, and McQuinn T, “Comparative in vitro study of bileaflet and tilting disk valve behavior in the pulmonary position.” *ASME J Biomechanical Engineering*, 2006. **128**(4):631-5.

Ilbawi MN, Lockhart CG, Idriss FS, DeLeon SY, Muster AJ, Duffy CE, and Paul MH, “Experience with St. Jude Medical valve prosthesis in children. A word of caution regarding right-sided placement.” *J Thorac Cardiovasc Surg*, 1987. **93**(1):73-9.

Kass DA, Yamazaki T, Burkhoff D, Maughan WL, and Sagawa D, “Determination of left ventricular end-systolic pressure-volume relationships by the conductance (volume) catheter technique.” *Circulation*. 1986. **73**:586-95.

Kawachi Y, Masuda M, Tominaga R, and Tokunaga K, “Comparative study between St. Jude Medical and bioprosthetic valves in the right side fo the heart,” *Jpm Cir. J*, 1991; **55**(6):553-62

Kilner PJ, et al, Pulmonary regurgitation: The effects of varying pulmonary artery compliance, and of increased resistance proximal or distal to the compliance, Int J Cardiol (2008), doi: 10.1016/j.ijcard.2008.06.078

Lankhaar JW, Westerhof N, Faes TJ, Gan CT, Marques KM, Boonstra A, Berg FG, Postmus PE, Vonk-Noordegraaf A, “Pulmonary vascular resistance and compliance stay inversely related during treatment of pulmonary hypertension.” *Eur Heart J*, 2008; **29**:1688-95.

Levick J, *An Introduction to Cardiovascular Physiology*. 1995, Oxford: Butterworth-Heinmann Ltd.

Losaw J, “In vitro Analysis of Prosthetic Heart Valves in the Pulmonary Position,” MS thesis. 2004, Clemson University.

Lurz P and Bonhoeffer P, "Percutaneous implantation of pulmonary valves for treatment of right ventricular outflow tract dysfunction." *Cardiol Young*, 2008. **18**(03):260-7.

Lurz P, Gaudin R, Taylor AM, and Bonhoeffer P, "Percutaneous Pulmonary Valve Implantation." *Seminars in Thoracic and Cardiovascular Surgery: Pediatric Cardiac Surgery Annual*, 2009. **12**(1):112-7.

McKay RG, Spears JR, Aroesty JM, Baim DS, Royal HD, Heller GV, Lincoln W, Salo RW, Braunwald E, and Grossman W, "Instantaneous measurement of left and right ventricular stroke volume and pressure-volume relationships with an impedance catheter." *Circulation*, 1984. **69**:703-10.

Mott R, *Applied Fluid Mechanics*. 2006, Upper Saddle River, New Jersey: Prentice Hall.

Mousseaux E, Tasu JP, Jolivet O, Simonneau G, Bittoun J, and Gaux JC, "Pulmonary arterial resistance: noninvasive measurement with indexes of pulmonary flow estimated at velocity-encoded MR imaging--preliminary experience." *Radiology*, 1999. **212**(3):896-902.

Nordmeyer J, Khambadkone S, Coats L, Scheivano S, Lurz P, Parenzan G, Taylor A, Lock J, Bonhoeffer P, "Risk stratification, systematic classification, and anticipatory management strategies for stent fracture after percutaneous pulmonary valve implantation." *Circulation*, 2007. **115**:1392-7

Reuben S, "Compliance of the human pulmonary arterial system in disease." *Circ Res*, 1971. **29**:40-50.

Rosendorff C, *Essential Cardiology: Principles and Practice*. 2001, New York: W.B. Saunders

Slife DM, Latham RD, Sipkema P, and Westerhof N, "Pulmonary arterial compliance at rest and exercise in normal humans." *Am J Physiol*, 1990. **258**(6.2):H1823-8.

Tesla N, *Valvular Conduit*. 1920: United States.

Tulevski II, Hirsch A, Dodge-Khatami A, Stoker J, van der Wall EE, and Mulder BJ, "Effect of pulmonary valve regurgitation on right ventricular function in patients with chronic right ventricular pressure overload." *Am J Cardiol*, 2003. **92**(1):113-6.

Weinberg CE, Hertzberg JR, Ivy DD, Kirby KS, Chan KC, Valdes-Cruz L, and Shandas R, "Extraction of pulmonary vascular compliance, pulmonary vascular resistance, and right ventricular work from single-pressure and Doppler flow measurements in children with pulmonary hypertension: a new method for evaluating reactivity: in vitro and clinical studies." *Circulation*, 2004. **110**(17):2609-17.

Westerhof N, Stergiopulos N, and Noble M, *Snapshot of Hemodynamics: An Aid for Clinical Research and Graduate Education*. 2005, Boston: Springer Science.

Womersley J, "Method for the calculation of velocity, rate of flow and viscous drag in arteries when the pressure gradient is known." *J Physiol*, 1955. **127**(3):553-63.

Yoganathan AP, He Z, and Jones SC, "Fluid mechanics of heart valves." *Annu Rev Biomed Eng*, 2004. **6**:331-62.